PNAS

31

Supplementary Information

2	
3	Single-molecule tracking reveals dual front door/back door inhibition of Cel7A
4	cellulase by its product cellobiose
5	
6	Daguan Nong ¹ , Zachary K. Haviland ¹ , Nerya Zexer ² , Sarah J. Pfaff ^{3,2} , Daniel J. Cosgrove ² , Ming Tien ⁴ ,
7	Charles T. Anderson ² , and William O. Hancock*1,5
8	
9	¹ Department of Biomedical Engineering, Pennsylvania State University, University Park, Pennsylvania,
10	USA
11	² Department of Biology, Pennsylvania State University, University Park, Pennsylvania, USA
12	³ Intercollege Graduate Degree Program in Plant Biology, The Pennsylvania State University, University
13	Park, Pennsylvania 16802
14	⁴ Department of Biochemistry and Molecular Biology, Pennsylvania State University, University Park,
15	Pennsylvania, USA
16	⁵ Department of Chemistry, Pennsylvania State University, University Park, Pennsylvania, USA
17	
18	* William O. Hancock.
19	Email: woh1@psu.edu
20	Author Contributions: D.N, Z.K.H, N.Z., M.T., C.T.A. and W.O.H. designed research; D.G. and Z.K.H.
21	performed research; S.J.P and D.J.C. contributed new reagents; D.G. and Z.K.H. analyzed data; D.N.,
22	C.T.A. and W.O.H. wrote the paper.
23	Competing Interest Statement: The authors declare that they have no known competing financial
24	interests or personal relationships that could have appeared to influence the work reported in this paper.
25	Classification: Biological Sciences; Plant Biology.
26	Keywords: Cel7A, cellulose, cellobiose, product inhibition, single-molecule tracking
27	
28	This PDF file includes:
29	Main Text
30	Figures 1 to 7

Abstract

Degrading cellulose is a key step in the processing of lignocellulosic biomass into bioethanol. Cellobiose, the disaccharide product of cellulose degradation, has been shown to inhibit cellulase activity, but the mechanisms underlying product inhibition are not clear. We combined singlemolecule imaging and biochemical investigations with the goal of revealing the mechanism by which cellobiose inhibits the activity of Trichoderma reesei Cel7A, a well-characterized exocellulase. We find that cellobiose slows the processive velocity of Cel7A and shortens the distance moved per encounter; effects that can be explained by cellobiose binding to the product release site of the enzyme. Cellobiose also strongly inhibits the binding of Cel7A to immobilized cellulose, with a K_i of 2.1 mM. The isolated catalytic domain of Cel7A was also inhibited to a similar degree by cellobiose, and binding of an isolated carbohydrate-binding module to cellulose was not inhibited by cellobiose, suggesting that cellobiose acts on the catalytic domain alone. Finally, cellopentaose inhibited Cel7A binding at micromolar concentrations without affecting the enzyme's velocity of movement along cellulose. Together, these results suggest that cellobiose inhibits Cel7A activity both by binding to the 'back door' product release site to slow activity and to the 'front door' substrate binding tunnel to inhibit interaction with cellulose. These findings point to new strategies for engineering cellulases to reduce product inhibition and enhance cellulose degradation, supporting the growth of a sustainable bioeconomy.

Significance

Cellulose, a polymer of repeating glucose subunits, is the primary component of plant cell walls. A promising route to reducing petrochemical use is digesting plant biomass to glucose and fermenting glucose to bioethanol. Cel7A is a model cellulase enzyme that degrades cellulose from one end to generate the disaccharide product, cellobiose. Because industrial-scale bioethanol generation generates high concentrations of cellobiose, product inhibition is a significant concern. We investigated product inhibition of Cel7A by cellobiose at the single-molecule level and found that cellobiose both slows the movement of Cel7 along cellulose and inhibits the initial binding of Cel7 to cellulose. These results suggest that cellobiose binds to the enzyme at more than one site and achieves its inhibition by multiple mechanisms.

Introduction

Cellulose, the most abundant biopolymer on earth, is a linear polysaccharide consisting of β -1,4-linked D-glucose units arranged in structurally repeating cellobiose units (1) that are released from cellulose during hydrolysis by cellulase enzymes. Because cellulose can be degraded into fermentable sugars for subsequent conversion to renewable fuels and other high-value products, it has enormous potential as a renewable source of energy and biomaterials (2). In nature, degradation of the cellulose polymer into cellobiose is carried out by extracellular cellulase enzymes secreted by fungi and bacteria (3). However, the β -1,4 bonds linking the sugar subunits in each cellulose chain are highly stable (4, 5), and the chains are tightly packed into partially crystalline microfibrils in which only a fraction of the chains lie on the microfibril surface and are thus accessible to enzymatic attack (2). This structure, coupled with the lignin and hemicellulose that surround cellulose in plant cell walls, makes lignocellulosic biomass highly resistant to enzymatic degradation. Intense research efforts are currently focused on improving the hydrolytic

degradation of lignocellulose, including advances in biomass pre-treatment technologies and schemes to improve the cellulolytic enzymes that catalyze the conversion of cellulose to fermentable sugars (6-14).

777879

80 81

82

83 84

85

86 87

75

76

An additional hurdle to cost-effective bioenergy production from plant biomass is that currently employed biomass-degrading enzyme systems are substantially inhibited by hydrolysis products including cellobiose and glucose (11, 14-18). Product inhibition retards the overall conversion rate of cellulose to the final glucose product and is particularly prominent at the high substrate loadings utilized industrially. Among biomass-degrading enzymes, Cel7A derived from the fungus, *Trichoderma reesei (Tr*Cel7A, hereafter Cel7A), is a prominent cellulase that has served as a model enzyme for several decades. Extensive investigations have demonstrated that Cel7A is inhibited by cellobiose (14, 17, 19), which is hypothesized to originate from the high binding affinity of cellobiose for the enzyme's product release site (20); however, experimental evidence supporting this hypothesis is limited.

88 89 90

91

92

93 94

9596

97

98

99

100

101102

103

104

105106

107

108109

Cel7A, which consists of a carbohydrate-binding module (CBM) and a catalytic domain (CD) containing a substrate-binding tunnel, hydrolyzes crystalline cellulose processively from the reducing end (Fig. 1 A) (21). The tunnel encompasses nine glucose subunits, which are numbered -7 to -1 preceding the active site and +1 and +2 in the product release site (Fig. 1A). Two exposed tryptophan residues, W40 and W376, are located at the tunnel's "front-door" (site -7) and the "backdoor" (site +1), respectively. The processive degradation cycle consists of hydrolysis of the β-1,4 glycosidic bond between the -1 and +1 subunits, expulsion of cellobiose from the product release site, and forward movement of the enzyme by two glucose subunits (~1 nm). Despite extensive study, the mechanism by which cellobiose inhibits Cel7A is not settled. Molecular dynamics simulations suggested a -14.4 kcal/mol free energy for cellobiose binding to the product release site, which corresponds to a 27 pM binding affinity (22). In contrast, functional assays have found half-maximal inhibition at cellobiose concentrations in the 1-20 mM range (23, 24). Numerous models for product inhibition of Cel7A have been put forward. Ståhlberg et al (16) found that added cellobiose had no effect on the adsorption of either the intact enzyme or the isolated carbohydrate-binding module to cellulose, whereas adsorption of the isolated catalytic domain was enhanced (rather than diminished) by cellobiose (16). Lee and Fan (25) suggested the product inhibition mechanism to be the deactivation of the substrate-adsorbed enzyme, a form of uncompetitive inhibition. In contrast, Holtzapple et al. (17) concluded that cellobiose inhibition was noncompetitive and suggested that cellobiose binds to a site that differs from the active site. Finally, Gruno et al. suggested a mixed-type inhibition with an apparent inhibition constant of 1.6 ± 0.5 mM (14).

110111112

113

114115

116

117

The lack of consensus regarding product inhibition of Cel7A is perhaps unsurprising based on the structures of Cel7A and cellulose. In a classical enzyme, the substrate and product binding sites are identical, and product inhibition results from competitive binding to the active site (26). In contrast, in Cel7A cellulose enters through the "front door" of the tunnel and cellobiose is released out the "back door" roughly 5 nm away, with the active site between (Fig. 1A) (20). Furthermore, in addition to the catalytic domain, Cel7A contains a CBM (Fig. 1A) that might facilitate the initial

binding of the enzyme to crystalline cellulose, enhance the affinity of the CD for cellulose, or have other functions (27, 28). Thus, among multiple non-exclusive mechanisms, cellobiose might inhibit Cel7A by interacting with the CBM and preventing binding of Cel7A to crystalline cellulose or by promoting dissociation of the CD from cellulose; it might bind to the front door in the catalytic domain to prevent threading of the cellulose chain into the tunnel; or it might bind to the "back door" product release site and thus block threading of cellulose into the active site. In solution studies, these different mechanisms would be expected to have complex effects on k_{cat} and K_M ; this complexity might help explain the diverse and conflicting hypotheses regarding product inhibition mechanisms for cellulases in previous work.

In contrast to studies in bulk solution that derive lumped parameters, single-molecule investigations can measure the processive velocity, run length, and other rate constants on individual enzyme molecules and thus provide novel insights into enzyme function. The goal of this study was to dissect the product inhibition mechanism of Cel7A by using single-molecule tracking to quantify the effect of cellobiose on the binding, processive movement, and dissociation of Cel7A from crystalline cellulose. In previous work, we found that Cel7A binds to and moves along cellulose in runs of ~30 nm at speeds of ~3 nm/s, corresponding to a hydrolysis rate of ~3 cellobiose units/s(29). These processive events were interspersed with numerous immotile episodes lasting tens of seconds, which may be due to the enzyme failing to find an exposed reducing end of a cellulose chain, being unable to extract a cellulose chain to cleave, or other mechanisms. Here, we find that cellobiose not only slows the processive velocity of Cel7A, which is expected, but also slows the landing rate of Cel7A on cellulose. Furthermore, cellobiose diminished the processive run length to a smaller degree than it slowed the velocity, meaning that binding durations were actually longer in the presence of cellobiose. These results suggest a model in which cellobiose inhibits Cel7A both by binding to the product release site to inhibit the forward progress of the enzyme, and also binding to the substrate binding tunnel to inhibit binding of the enzyme to its cellulose substrate.

Materials and Methods

Isolation of *Gluconacetobacter xylinus* (acetobacter) cellulose and quantum dot (Qdot) labeling of Cel7A (Sigma-Aldrich; Cas: E6412-100UN) were carried out as previously reported (29) on a custom-built microscope, described previously (30). Isolated Cel7A CD (generously provided by Stephen R. Decker, NREL) was expressed and purified as detailed previously (31) and subsequently biotinylated and Qdot labeled using the same protocol as that of Cel7A. Cellobiose was obtained from Sigma (Sigma-Aldrich; Cas: 528-50-7). To investigate the activity of Cel7A on acetobacter cellulose as a function of cellobiose concentration, we adsorbed cellulose to plasmacleaned glass coverslips by spreading 20 µL of 2.54 mM cellulose on a coverslip, drying it in the oven for 2 min, and assembling a flow cell using double-sided tape. Following cellulose adsorption, surfaces were blocked to minimize nonspecific adsorption by flowing 1 mg/mL bovine serum albumin into the flow cell for 5 min, followed by an enzyme solution consisting of 2 nM Cel7A labeled with 0.5 nM Qdot (Thermo Scientific; Cas: Q10143MP), 5 mM dithiothreitol, and 0 to 16 mM cellobiose in 50 mM sodium acetate buffer, pH 5.0. The enzyme solution was mixed for 5 min

before being added to the flow cell. The Qdot525-labeled Cel7A was imaged by a total internal reflection fluorescence microscope (TIRFM) using a 405 nm laser (50 mW) on a custom-built microscope (30). TetraSpeckTM beads (Thermo Scientific; Cas: T7279) were imaged simultaneously as fiduciary markers to compensate for stage drift. Surface-immobilized cellulose was imaged by interference reflection microscopy (IRM), as described (29, 30). Recording of movies began immediately before the enzyme solution was added to the flow cells. Adsorption of Cel7A or CBM3-A488 (32) to the surface of the cellulose (Fig. 2A) was measured by counting bright dots using the "Find Maxima" plugin in ImageJ; prominence was set to 25 for Qdot525-labeled Cel7A and 10 for the Alexa488-labeled CBM3-A488, respectively. In every field of view, the fraction of the area occupied by cellulose was quantified using ImageJ by applying a threshold on the IRM images. The number of enzymes per screen were normalized to the area per screen occupied by cellulose (described in Fig SI. 2). Analysis of Cel7A velocity and run length was as described previously (29). All experiments were performed at 21° C.



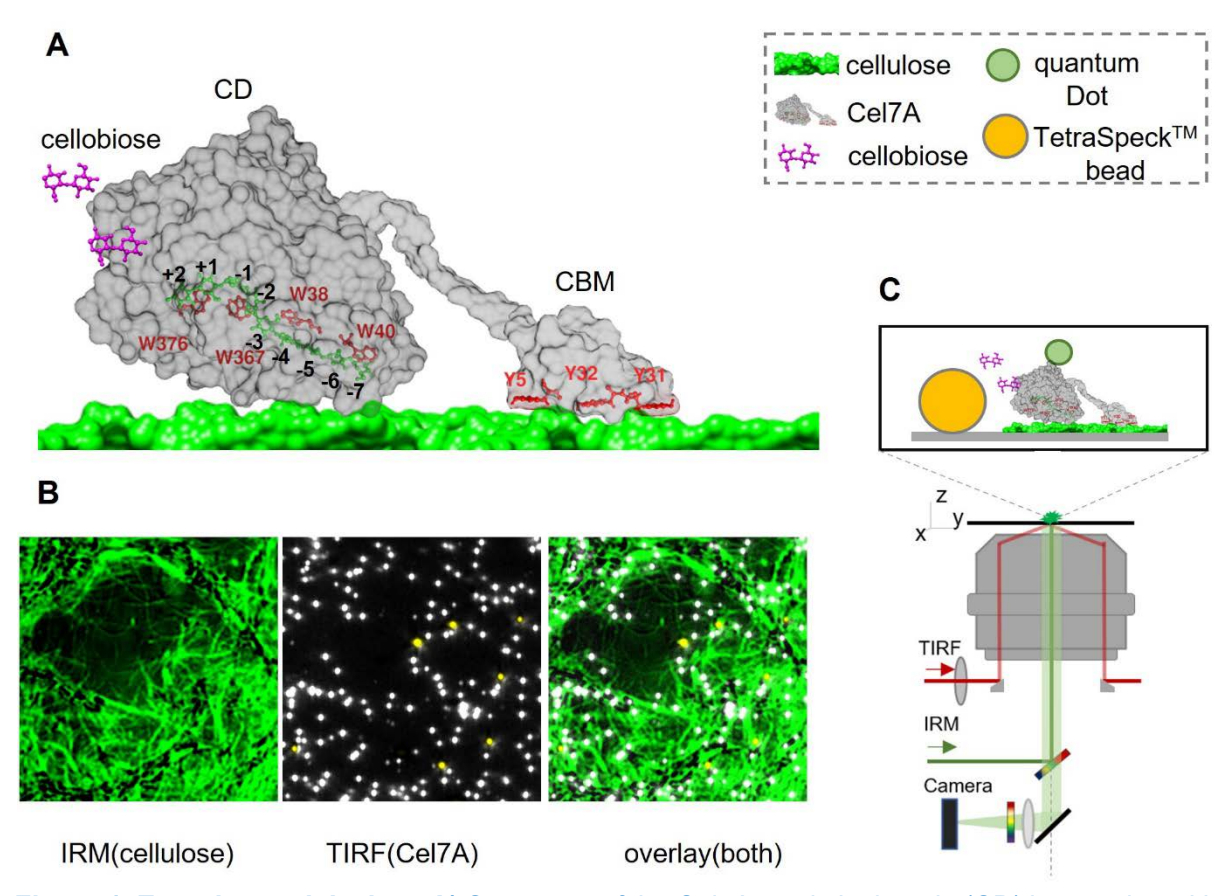


Figure 1, Experimental design. A) Structures of the Cel7A catalytic domain (CD) in complex with a cellulose chain (left, PDB code 8CEL) and the cellulose-binding module (CBM; right, PDB code 1CBH). The linker connecting the two domains is drawn by hand. **B)** The surface-immobilized cellulose is imaged by IRM (green strands), Cel7A enzymes (labeled with Qdot525, bright objects) and TetraSpeck beads (yellow dots) are imaged by TIRFM. **C)** Experimental design of Qdot-labeled Cel7 interacting with surface-immobilized cellulose in presence of soluble cellobiose (not to scale); the yellow sphere is TetraSpeck fiduciary marker (29, 30).

Results

186187

184

185

188

189190

191

192

193194

195

196

197198

199

200

201

202

Cellobiose decreases the binding affinity of Cel7A to cellulose

To investigate the mechanism of inhibition of Cel7A by cellobiose, we used a previously described single-molecule microscopy assay, in which quantum dot (Qdot)-labeled Cel7A enzymes are visualized landing and moving along bacterial cellulose (29). The surface-immobilized cellulose is imaged by Interference Reflection Microscopy (IRM; Fig. 1B) and the Qdot-labeled Cel7A is imaged by Total Internal Reflection Fluorescence microscopy (TIRF). Upon introducing 2 nM Qdotlabeled Cel7A into a flow cell containing immobilized cellulose, the number of enzymes on the surface increased over time and reached a steady state after roughly 200 seconds (Fig. 2A). We first asked whether cellobiose inhibits the binding of Cel7A to its cellulose substrate. To address this question, we flushed Cel7A into flow cells in the presence of increasing concentrations of cellobiose and monitored the accumulation of bound enzymes on the surface, where the number of surface-bound Cel7A at steady-state reflects a balance of on-rate and off-rate. The steady-state number of bound enzymes decreased progressively with increasing [cellobiose] (Fig. 2B). Each timecourse was fit by a rising exponential function, and the steady-state accumulation as a function of [cellobiose] was well fit by a simple inhibition model with a K_I of 2.3 mM cellobiose (Fig. 2C). The time constant for the rising exponential was independent of [cellobiose] (Fig. 2C inset), a point that we will discuss below.

203204205

206

207

208

209

210211

212

213

214

Like other cellulases, Cel7A is a modular protein with a N-terminal catalytic domain and a C-terminal carbohydrate binding module (CBM) connected through a polypeptide linker domain (Fig. 1). Thus, Cel7A can potentially bind to cellulose through its catalytic domain, its carbohydrate binding module, or both. As such, cellobiose might inhibit the binding of Cel7A to cellulose by interfering with CBM and/or catalytic domain binding. To test whether the binding inhibition by cellobiose is mediated through the catalytic domain, we repeated the assay using an isolated Cel7A catalytic domain (31). The binding timecourse of the isolated CD was similar to intact Cel7 and cellobiose inhibited binding in a similar manner, with a K_I of 3.0 mM cellobiose (Fig. 2D and E). Thus, we conclude that cellobiose inhibits Cel7A binding to cellulose by acting through the catalytic domain.

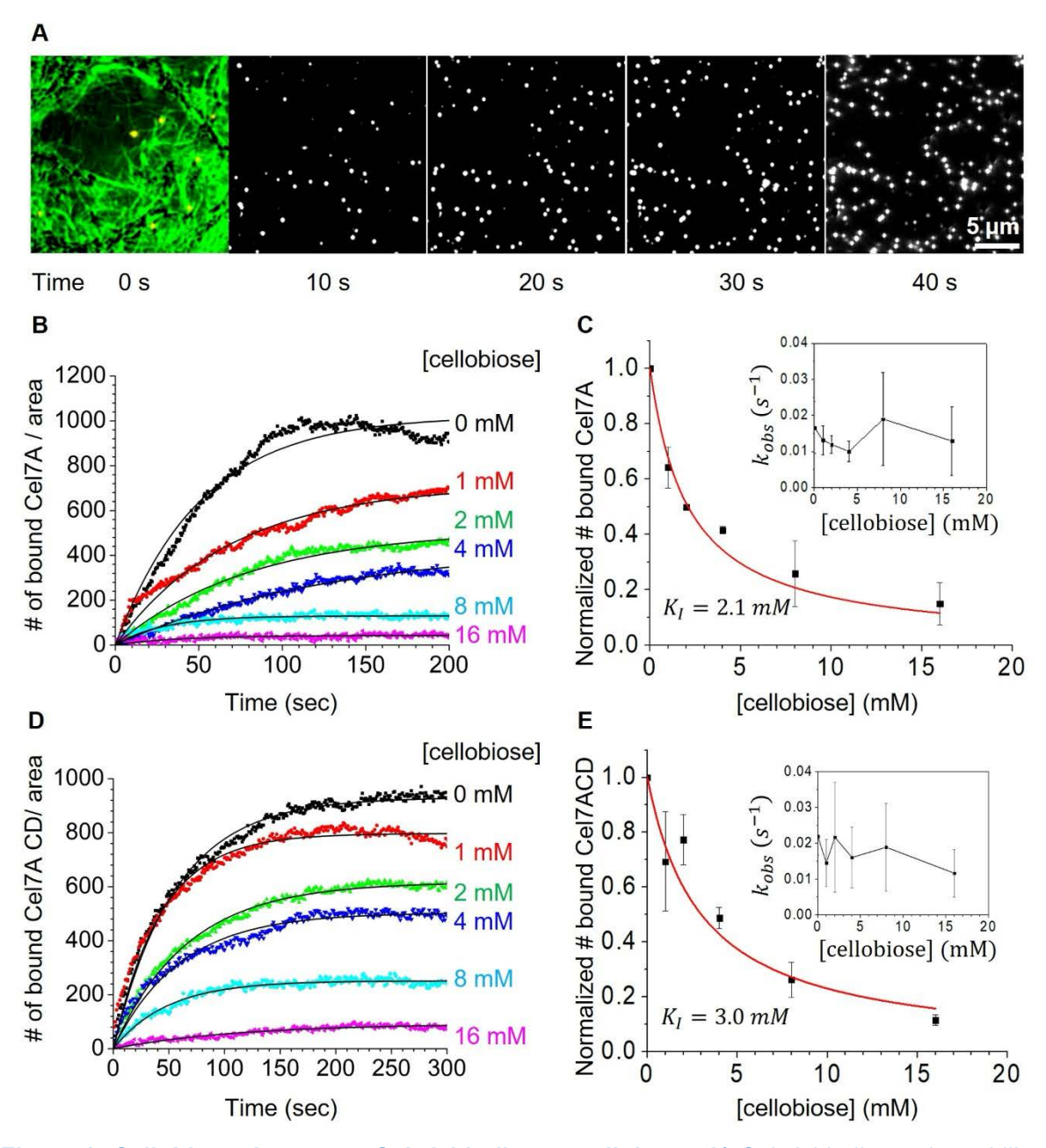


Figure 2, Cellobiose decreases Cel7A binding to cellulose. A) Cel7A binding to immobilized cellulose. Image at 0 s shows cellulose substrate (green) imaged by IRM, and TetraSpeck bead fiduciary markers (yellow) imaged by fluorescence. Subsequent images show bound Cel7A (white dots) imaged at 10 s intervals, showing accumulation over time. **B)** Numbers of Qdot-labeled Cel7A enzymes bound to surface-immobilized cellulose over time with increasing [cellobiose] from a representative experiment. Values represent numbers of particles per 75 μm by 75 μm screen, with values normalized to the proportion of each screen covered by cellulose. Binding timecourse data were fit by single exponentials (thin black curves), $Cel7A_{bound}(t) = Cel7A_{bound}SS*$ $(1 - e^{-k_{obs}*t})$. See Supplementary Figs. 2 and 3 for experimental details. **C)** Steady-state $Cel7A_{bound}$ as a function of [cellobiose]. Data come from three independent datasets, where each is normalized to steady-state $Cel7A_{bound}$ in the absence of cellobiose and error bars represent the standard deviation of three datasets collected on different days. Data are fit by a competitive

inhibition model with $Cel7A_{Bound} = 1/$ (1+ $[cellobiose]/K_I$), where $K_I = 2.3$ mM cellobiose. Inset, the observed rate constant k_{obs} against [cellobiose]. **D and E)** Binding kinetics and steady-state binding values for isolated Cel7A catalytic domain, following identical methods to the intact Cel7A in panels B and C. All fit parameters and errors are given in Supplementary Table 6.

Cellobiose decreases the processive velocity and run length of Cel7A on cellulose

228229

230

231

232

233234

235

236

237238

239

240241

242

243

244

245

246

247

248249

250

251

252

253

254255

256257

We next investigated how cellobiose affects the movement of Cel7A molecules bound to immobilized cellulose. Previously, Cel7A molecules were found to interact with cellulose either in a static state or in a processive manner in which they moved intermittently along the cellulose before stopping or dissociating from the surface (29). These processive movements can be seen in example x-y and distance-time traces of moving Cel7A molecules in the absence or presence of 16 mM cellobiose (Fig. 3A&B). In analyzing processive movements, we defined a moving Cel7A molecule as one that moved at least 10 nm over a duration of at least 5 s, and to avoid false positives due to stage drift, we defined a minimum velocity cutoff of 0.5 nm/s. In the absence of cellobiose, the mean velocity was 4.3 ± 4.9 nm/s (mean ± SD, N = 551 trajectories) and the run length was 39.7 ± 45 nm (mean ± SD, N = 551 trajectories), where the removal of each cellobiose unit corresponds to ~1 nm displacement (33). At 16 mM cellobiose, the distributions of both the velocity and run length were shifted to lower values (Fig. 3C&D): the mean velocity was 1.3 ± 1.7 nm/s (mean \pm SD, N = 502 trajectories) and the run length was 25.1 \pm 20.7 nm (mean \pm SD, N = 502 trajectories). When velocity was plotted as a function of [cellobiose], the data were well fit by a simple inhibition model with a K_I of 2.3 mM cellobiose (Fig. 3E). Similarly, Cel7A run length (defined as the distance moved during processive segments) was diminished by cellobiose, with a K_I of 2.6 mM cellobiose (Fig. 3F). However, both inhibition models included an offset, meaning that the velocity was inhibited by a maximum of 75%, whereas run length was inhibited by a maximum of 30%. Thus, cellobiose had a stronger impact on processive velocity than it did on processive run length. Similar to the landing rates, the velocity and run length of isolated Cel7A catalytic domain were similar to the intact enzyme, as was the effect of cellobiose on velocity and run length (Fig. 3G and H).

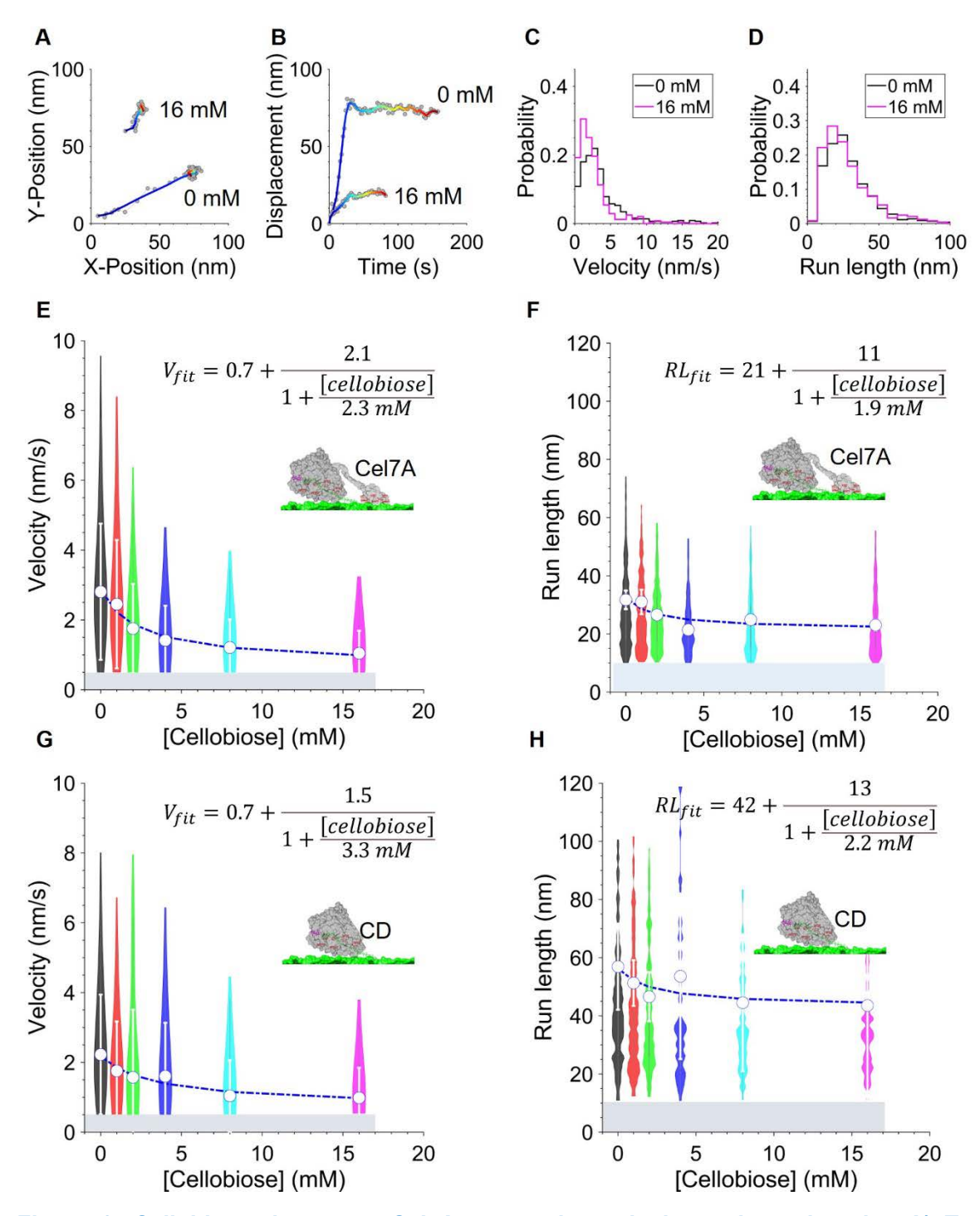


Figure 3, Cellobiose decreases Cel7A processive velocity and run length. A) Typical trajectories of Cel7A on the cellulose surface under control and 16 mM cellobiose conditions. Time is color-coded, starting from blue and ending in red. **B)** Distance from origin versus time for the same Cel7A molecules. Additional raw traces are provided in Supplementary Figures 12-15. **C, D)** Distributions of processive velocity **(C)** and run length **(D)** at zero (N = 565) and 16 mM (N = 504) cellobiose concentrations. **E)** Processive velocity of Cel7A as a function of [cellobiose], with fit to a simple inhibition model. Gray bar denotes minimum measurable velocity of 0.5 nm/s. **F)** Processive run length of Cel7A as a function of [cellobiose]. Gray bar denotes minimum

measurable run length of 10 nm. **G and H)** Velocity and run length of isolated Cel7A catalytic domain in the presence of varying [cellobiose]. Velocity and run length distributions are given in Supplementary Figures 6 and 7, and fit parameters with errors are given in Supplementary Table 1.

271272273

274

275

276277

278279

280

281

282

283284

285

286

287288

289

267

268

269270

Cellobiose does not promote dissociation of Cel7A from cellulose

The reduction by cellobiose in the steady-state number of bound Cel7A (Fig. 2) could result from either a reduction in the on-rate for Cel7A binding to cellulose, an increase in the off-rate of the enzyme from cellulose, or both. To address this question, we analyzed the duration of static and processive binding events at increasing cellobiose concentrations. For consistency, we used a lower limit of 10 s for both static and processive events. For both static and processive populations, the dwell time that Cel7A was bound to cellulose before dissociation increased slightly with increasing [cellobiose] (Fig. 4A&B). Thus, there is no evidence that the off-rate, defined as the inverse of dwell time, was enhanced by cellobiose. To better understand the effects of cellobiose when the enzyme is actively moving and thus presumably digesting the cellulose, we plotted the duration of processive segments, defined as the run length divided by the velocity. Processive duration increased with increasing [cellobiose] (Fig. 4D). This enhanced duration can be explained by the strong reduction in velocity by cellobiose, (see Fig. 3C) with only a moderate reduction in the run length (see Fig. 3D). Consistent with data for purely static molecules, the duration of static segments that occurred between processive segments for enzymes that moved processively (e.g. Fig. 3A&B) also increased slightly at elevated [cellobiose] (Fig. 4C) (29). Thus, we observed no evidence that cellobiose increases the off-rate of Cel7A from cellulose, and instead the off-rate appeared to slow somewhat with increasing [cellobiose].

290291292

293294

295

296297

298

299

The lack of an effect of cellobiose on the Cel7A off-rate is consistent with a model in which cellobiose inhibits the binding of Cel7A to cellulose. From Fig. 2, the number of bound Cel7A molecules at steady-state decreased at elevated [cellobiose]. By definition, at steady-state the rate of enzymes binding to the surface is equal to the rate of enzymes leaving the surface. Thus, because the off-rate is unaffected by cellobiose, we conclude that the reduction in the steady-state bound population must result from a decrease in the Cel7A binding rate (developed further in Supplementary Information). These data together suggest that cellobiose acts on Cel7A as a competitive inhibitor of cellulose binding.

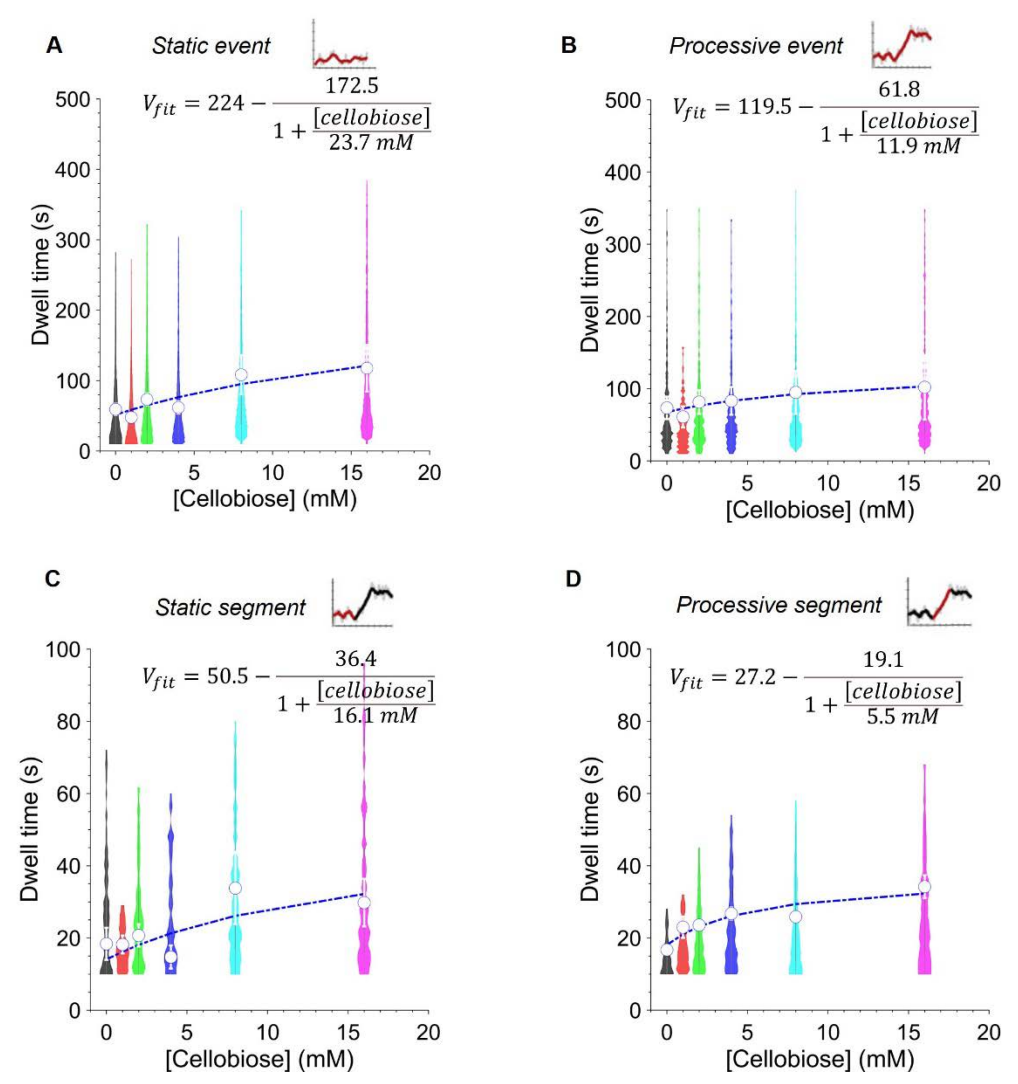


Figure 4, Effect of cellobiose on dwell times of Cel7A in different phases of engagement with cellulose. A) Dwell times of Cel7A static binding events, defined as binding events of duration ≥10 s with displacement <10 nm. B) Dwell times of processive events, defined as landing events that contain at least one processive segment with displacement >10 nm over at least 10 s. C) Dwell times of processive segments, with dwell time calculated as run length/velocity. D) Dwell times of static segments that occurred before or after processive segments during processive events. All plots show populations with fits to exponential distribution as open circles. Insets show schematic of the distance from origin versus time, with the segments of interest highlighted in red. Curves were fit to a product inhibition model in which cellobiose elongates the dwell times. For panel A, the curve was constrained by $K_{\rm I} \le 16~{\rm mM}$ to allow convergence of the fit; thus, 16 mM is a lower bound. Full dwell time distributions are given in Supplementary Figures 8-11, all fit parameters and associated errors are given in Supplementary Tables 2-5, and corresponding dwell time plots for Cel7A CD are given in Supplementary Figure SI 4.

Cellobiose does not affect the binding of a CBM domain to cellulose

To test whether cellobiose inhibits binding by a CBM domain, we measured the binding kinetics of CBM3-A488, a recently characterized AlexaFluor488 labeled CBM3a fragment from *Clostridium*

thermocellum (32). We were unable to express an isolated CBM domain from Cel7A due to technical limitations. However, because CBM3-A488 contains key conserved tryptophan residues at its cellulose binding interface (Fig. 5A), determining how cellobiose affects its binding to cellulose is relevant to determining whether cellobiose is acting solely on the catalytic domain of Cel7A. The binding rate of CBM3-A488 to immobilized cellulose was considerably faster than Cel7A, reaching steady-state within roughly 15 s (Fig. 5). Importantly, the steady-state number of bound CBM3-A488 molecules was unaffected by either 50 mM cellobiose or 50 µM cellopentaose. Furthermore, no detectable diffusion of the CBM on the immobilized cellulose was observed. Extrapolating this CBM3-A488 result to the CBM1 domain of Cel7A, together with the finding that isolated Cel7A CD is blocked by cellobiose, we conclude that cellobiose slows Cel7A binding to cellulose by acting on the catalytic domain of the enzyme rather by inhibiting binding through the CBM.

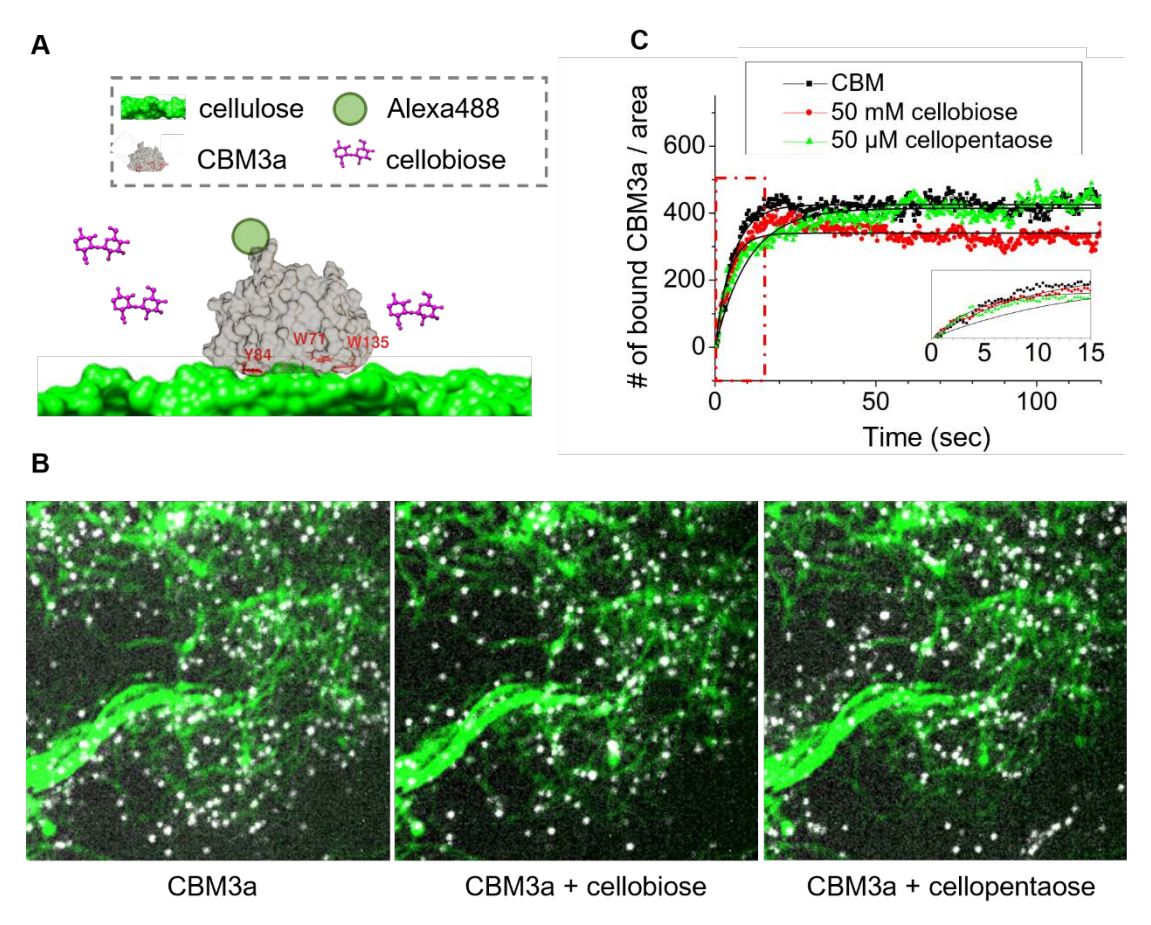


Figure 5, The binding of an isolated CBM to cellulose is unaffected by either cellobiose or cellopentaose. A) A model of CBM3a (PDB code: 4JO5) binding to cellulose, showing the location of tryptophan and tyrosine residues implicated in binding. B) Steady-state accumulation of 10 pM Alexa488-labeled CBM3-A488 on cellulose under control conditions (left) and in the presence of 50 mM cellobiose (middle) and 50 μM cellopentaose (right). Cellulose imaged by IRM is shown in green, and CBM3-A488 imaged by TIRF is shown in white. C) Time course of CBM3-A488 accumulation on cellulose, showing similar landing rate and total number of bound enzymes for the three conditions. Fluctuations at the plateau are within experimental error. Inset shows early landing events. Fit parameters and errors are given in Supplementary Table 8.

Cellopentaose slows the landing rate of Cel7A without affecting its velocity

 How might cellobiose inhibit binding of Cel7A to cellulose? One potential mechanism is that cellobiose binds in or near the substrate binding tunnel, the front door, and competitively inhibits the entry of a cellulose chain into the tunnel. If this were the only mode of inhibition (independent of cellobiose binding to the product release site), it should affect the landing rate only and not the velocity. A prediction of this "front door binding" model is that a longer polysaccharide, such as cellopentaose, which can fit into the entrance to the substrate binding tunnel, but which is presumably too large to fit into the product release site, should affect the Cel7A landing rate without affecting the velocity. To test this prediction, we analyzed Cel7A in the presence of increasing concentrations of cellopentaose and repeated the binding rate and enzyme motility analyses we performed for cellobiose. As seen in Fig. 6A&B, cellopentaose inhibited the Cel7A landing rate on cellulose, similar to cellobiose but with a K_I of 1.1 μ M, more than 1000-fold tighter than cellobiose. This smaller K_I is consistent with the longer cellopentaose interacting with more residues in the substrate binding tunnel to achieve a higher binding affinity. In contrast with the landing rate, Cel7A velocity and processive run length were unaffected by cellopentaose (Fig. 6C&D).

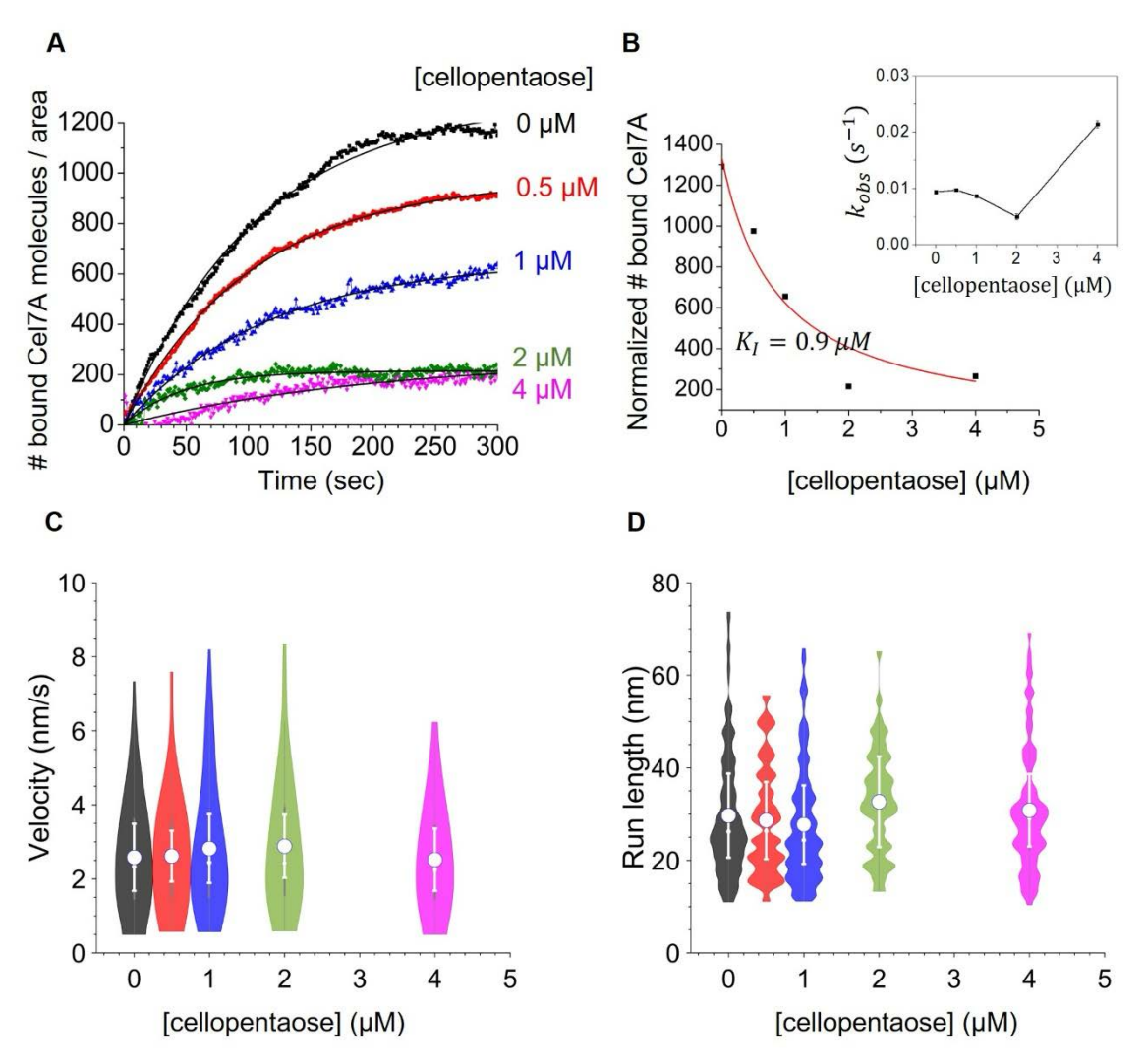


Figure 6, Cellopentaose decreases Cel7A binding to cellulose without affecting the velocity and run length. A) Timecourse of the number of Qdot-labeled Cel7A enzymes accumulating on the cellulose surface in the presence of cellopentaose. B) Steady-state $Cel7A_{bound}$ as a function of [cellopentaose]. Steady-state $Cel7A_{bound}$ are normalized to control condition in the absence of cellopentaose and are fit by a competitive inhibition model $Cel7A_{Bound} = 1/(1 + [Cellopentaose] / K_I)$, where $K_I = 1.1 \, \mu \text{M}$ cellopentaose. Fit parameters and errors are given in Supplementary Tables 7 and 9. Inset: rate constants from exponential fits. (C, D) Processive velocity and run length as a function of [cellopentaose], showing a lack of inhibition of processive degradation once the enzyme has landed on cellulose.

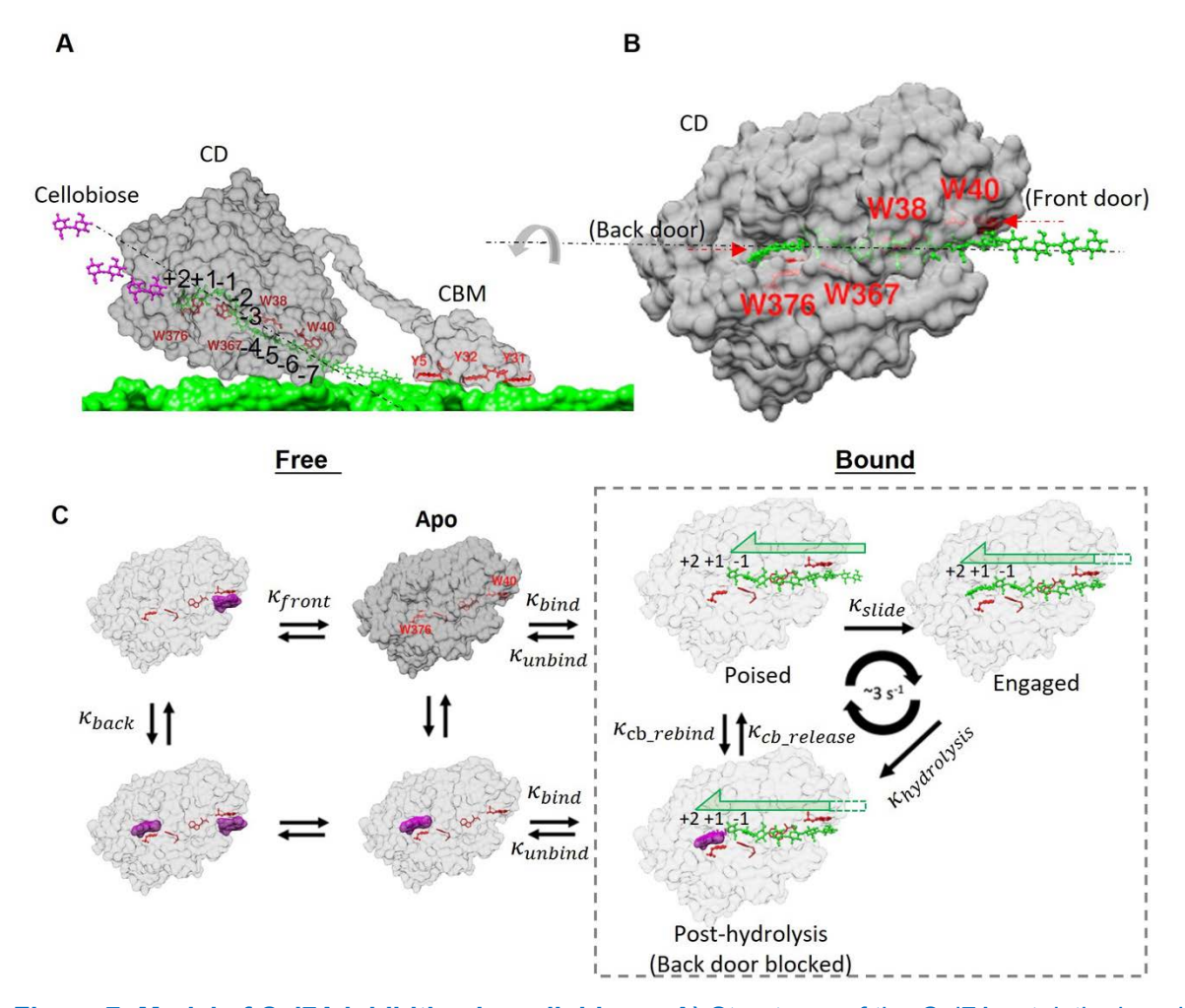


Figure 7: Model of Cel7A inhibition by cellobiose. A) Structures of the Cel7A catalytic domain (CD; PDB code 8CEL) in complex with a cellulose chain, the cellulose-binding module (CBM; PDB code 1CBH) adsorbed to the crystalline cellulose lattice, and cellobiose (purple) being released from the product binding site. B) The catalytic domain is rotated to show entrance of the substrate binding tunnel at the -7 site. C) Proposed model of Cel7A inhibition by cellobiose. Free Cel7A in solution ($Apo\ state$) binds to an exposed reducing end of a cellulose strand with rate k_{bind} to enter the *Poised state* in which the product release site is empty. Cel7A slides forward at rate k_{engage} to enter the *Engaged state* in which the strand is positioned in the active site of the enzyme. Hydrolysis of the cellulose strand at rate $k_{hydrolysis}$ generates cellobiose in the active site, and cellobiose is released at rate $k_{cb_release}$ to complete the processive cycle. This processive cycle occurs at ~3 s⁻¹ and results in a 1 nm displacement of the enzyme. Cellobiose (purple) can inhibit binding of Cel7A to cellulose by binding to the front door of the enzyme (k_{front}); the apparent binding constant, K_I is 2.1 mM based on Fig. 2C. Cellobiose can slow the catalytic cycle by binding to the product release site of Cel7A in the *Poised state* (k_{cb_rebind}) thus inhibiting forward sliding; the K_I for slowing the catalytic cycle is 2.3 mM based on Fig. 3E.

Discussion

By quantifying at the single-molecule level how cellobiose alters the landing, processive movement, and dissociation of Cel7A from cellulose, we gain new insights into the mechanism of cellulose degradation by Cel7A. The key results were that cellobiose inhibits cellulose binding of both intact Cel7A and the isolated catalytic domain, and that cellulose inhibits the processive velocity and to a lesser degree the processive run length of Cel7A. We interpret our results in the context of a model of cellulose binding and digestion by Cel7A shown in Fig. 7.

A unique aspect of processive glucoside hydrolases like Cel7A is that their substrate, a cellulose chain, is threaded through the enzyme to the active site, thus separating the sites of substrate binding and product release. Enzymes that release products through a different route than they bind their substrates have been termed "back door" enzymes, with examples including acetylcholinesterase, myosin and actin (34-36). By this definition, Cel7A is a back door enzyme; the substrate binding channel is the front door, with tryptophan W40 being a key mediator of substrate binding (Fig. 1A) (20), and the product release site is the back door, where tryptophan W376 has been proposed as a key mediator of cellobiose binding (Fig. 1A) (8, 20). This front door/back door structure makes it difficult to infer the mechanism of product inhibition from bulk solution studies alone, and emphasizes the need for single-molecule approaches to uncover the specific steps in the enzymatic cycle that are altered by cellobiose.

We propose that cellobiose slows the velocity of Cel7A by reversibly binding to the product release site and inhibiting the forward movement of the enzyme along cellulose (Fig. 7). Because Cel7A is processive and remains bound to cellulose before and after product release, inhibition of its velocity by cellobiose is expected to be non-competitive. The 2 mM K_I for inhibition of velocity agrees with previous results from bulk solution studies (23, 24), although it diverges from Molecular Dynamics simulations that predict the affinity of cellobiose for the product release site to be 28 pM (based on a Δ G of -14.4 kcal/mol (22)), and isothermal calorimetry experiments that measured a 19 μ M affinity for cellobiose binding to *Talaromyces emersonii* Cel7A (11). How can we reconcile a micromolar cellobiose affinity in solution with a mM observed inhibition constant for processive velocity? One possibility is that the presence of a cellulose chain in the substrate tunnel allosterically lowers the affinity of the product release site for cellobiose, and this conformation is not accessed in the published experiments and simulations of cellobiose binding to Cel7A. An alternate explanation is that following product release, threading of the chain into the active site is strongly favored kinetically and/or thermodynamically over binding cellobiose from solution, thus requiring high [cellobiose] to inhibit an active enzyme.

One outstanding question regarding the processive mechanism of Cel7A is: What terminates a processive run of Cel7A? Our mean Cel7A run length of ~30 nm is approximately an order of magnitude shorter than the estimated ~300 cellobiose equivalents chain length of bacterial cellulose (37), implying that processive runs are not terminated by the enzyme reaching the end of a strand. It has been proposed that processivity is terminated by roadblocks in the form of other enzymes or features of the cellulose substrate (38, 39), and one interpretation of our shorter run length in the presence of cellobiose (Fig. 4) is that cellobiose is enhancing existing roadblocks or acting itself as a roadblock. However, it is notable that, because cellobiose reduced the velocity

to a greater extent than the run length, both the duration of processive segments and the overall dissociation rate of the enzyme from cellulose were slower in the presence of cellobiose (Fig. 4). This slowing is relevant when considering the third potential termination mechanism: cellulose chain dethreading (40) from the substrate binding tunnel.

435 436 437

438 439

440

441442

443

444

445446

447

448

449

450

451

432

433 434

> Fig. 7 presents a framework for interpreting potential mechanisms by which cellobiose reduces the velocity and run length of Cel7A. Starting from the unbound Apo state, the enzyme threads a cellulose chain into the substrate binding tunnel to reach the Poised state. Further threading of the terminal cellobiose subunit into the active site results in an Engaged state, cleavage of the terminal cellobiose leads to the Post-hydrolysis state, and release of the cellobiose product returns the enzyme to the Poised state that begins the next cycle. Slowing of the Cel7A velocity by cellobiose can be easily interpreted in this framework as reversal of the product release step, such that in the presence of cellobiose the enzyme spends a greater fraction of its cycle in the Posthydrolysis state. However, if processive runs are terminated by the cellulose chain unthreading from the substate binding tunnel in the Post-hydrolysis state, then cellobiose should lead to faster dissociation rather than slower dissociation from cellulose. One potential mechanism that can account for the finding that the processive dwell time increases, rather than decreases in the presence of cellobiose (Fig. 4D) is that Cel7A dissociates only from the Poised state and not from the Post-hydrolysis state. In this way, cellobiose would act as an uncompetitive inhibitor in that it enhances binding of the enzyme to the cellulose substrate by slowing dissociation from the cellulose substrate.

452453454

455

456

457

458 459

460

461

462

463

464

465

466

467

468

469

470471

472

473474

One unexpected finding was that the binding of Cel7A to cellulose was diminished at increasing cellobiose (and cellopentaose) concentrations. Binding of Cel7A to crystalline cellulose involves a multi-step process of binding to the cellulose surface (through either the catalytic domain or carbohydrate binding module), finding a free reducing end, and the enzyme threading the chain into the substrate tunnel to fully engage with the substrate. This binding process is simplified into the single substrate binding step in Fig. 7. The slowing of Cel7A binding kinetics by cellobiose can be seen by comparing the landing rate curves to the dwell time curves. With elevated [cellobiose], the dwell time did not shorten, and instead was slightly longer (Fig. 4). Thus, the Cel7A off-rate, which is calculated by inverting the dwell time, was not enhanced at elevated [cellobiose]. Turning to the landing rate data in Fig. 2, we can see that the steady-state population of bound Cel7A decreased strongly with increasing [cellobiose], whereas the observed rate constant describing the exponential rise to the steady-state plateau did not change. The decrease in the plateau without any change in the rate constant of accumulation is surprising, because in a standard twocomponent equilibrium, the exponential rate constant that describes the response of a perturbation (flushing the Cel7A into the flow cell in this case) generally involves both the forward and reverse rate constants (41). However, as described in Supplementary Information, both the cellulose binding sites and the number of Cel7A enzymes are in excess under the conditions of the experiment. In this special case, the steady-state plateau is proportional to $k_{on} * [Cel7A]/(k_{on} *$ $[Cel7A] + k_{off}$), whereas the accumulation rate is determined solely by the off-rate, k_{off} . From this analysis, we conclude that cellobiose affects only the on-rate of Cel7A for cellulose and not the off-rate.

How does cellobiose inhibit on-rate for Cel7A binding to cellulose? In principle cellobiose could act at five possible sites: the CBM, the product release site (back door), the substrate binding tunnel (front door), elsewhere on the catalytic domain, or by binding directly to cellulose (Supplementary Figure 5). We rule out the CBM by our finding that the isolated catalytic domain binding is inhibited by cellobiose to a similar extent as the intact enzyme (Fig. 2 and Fig. 3). A back door mechanism is opposed by two arguments. First, the product release site (+1 and +2 in Fig. 7A) is on the opposite side of the catalytic domain from the substrate binding tunnel entrance (-7 in Fig. 7). Second, cellopentaose inhibits the landing rate without affecting the velocity (Fig. 6), and the fact that these two activities are separable argues against a single-site mechanism regulating both the velocity and the binding rate. In contrast to these first two mechanisms, our data do not rule out the possibility that cellobiose inhibits Cel7A binding by interacting directly with cellulose and blocking adsorption of Cel7A. However, due the chemical similarity between cellobiose and cellulose, the affinity of cellobiose for cellulose should be similar to the selfassociation of cellobiose, and the high solubility of cellobiose suggests that this affinity is much weaker affinity than the mM inhibition constants observed here. Our data also don't rule out the possibility that cellobiose binds to a cryptic allosteric site on Cel7A and blocks cellulose binding either directly or allosterically; however, there is no evidence in the literature for such a site. Thus, our favored model is that cellobiose binds to the substrate binding tunnel of Cel7A (the front door) and acts as a competitive inhibitor for cellulose binding (Fig. 7). Specific binding to this site is consistent with the chemical similarity between cellobiose and the cellulose chain that the tunnel has evolved to bind tightly. Furthermore, the finding that cellopentaose inhibits cellulose binding with a much lower K_i is consistent with this longer polymer occupying a larger portion of the tunnel and hence binding more tightly.

475476

477

478

479 480

481 482

483

484 485

486

487

488 489

490

491 492

493

494

495 496

497

498499500

501502

503

504

505506

507

508509

510

511

512513

514515

516

517

Our results suggest that the disparate conclusions in the literature regarding the mechanism of product inhibition of Cel7A arise from two factors: first, Cel7A is a processive enzyme that acts on an insoluble substrate and thus likely differs from classical models of enzyme inhibition, and second, cellobiose binds to at least two separate sites on the enzyme. Cellobiose binding to the front door of the substrate binding tunnel is a form of competitive inhibition, which is expected to raise the K_M for cellulose and have no effect on the k_{cat} . In contrast, cellobiose binding to the product release site is expected to slow the k_{cat} , which in its simplest form is noncompetitive inhibition. However, because cellobiose slows Cel7A velocity to a greater degree than it decreases run length (Fig. 3E & F), the Cel7A off-rate is slowed somewhat by cellobiose, which is expected to decrease the K_M , a hallmark of uncompetitive inhibition. Using the steady-state accumulation data in Fig. 2C together with the velocity data in Fig. 3E, we simulated expected results from a bulk biochemical assay at varying [cellobiose]. We found that the simulated data fit a mixed inhibition model, with the k_{cat} decreasing and K_M increasing with increasing [cellobiose] (Supplementary Data).

How can these new insights into Cel7A product inhibition help efforts to more cost-efficiently convert lignocellulosic biomass to bioethanol? One clear direction is to explore engineered Cel7A with mutations in the substrate binding tunnel and product release site that reduce the affinity for

cellobiose without inhibiting binding or hydrolysis of cellulose. To that end, mutating W40 in the front door of the substrate binding tunnel was found to increase the K_M for cellulose by a factor of two, while also having the added benefit of increasing the k_{cat} (6, 42). A promising avenue for future work will be exploring the degree to which product inhibition is diminished in this and other mutations located in the substrate tunnel. In principle, an even more promising direction is to mutate residues around the product release site to reduce cellobiose affinity at the back door. However, a published study that explored a large number of back door mutants found that, although some mutations (including the equivalent of W376A; Fig. 1A) did reduce the extent of product inhibition, they also all diminished the overall turnover rate of the enzyme (11). One implication of the current results is that mutations at the front door are expected to alter the effect of cellobiose on the K_M of Cel7A for cellulose, whereas mutations to the back door are expected to alter the effect of cellobiose on the k_{cat} . A final implication of the current work is that product inhibition does not appear to act through the carbohydrate binding domain, and as such, further engineering of that domain appears less promising than the catalytic domain. Together, these results point to new directions for engineering cellulases as critical components of lignocellulose processing in a sustainable bioeconomy.

Acknowledgements

518

519

520521

522

523

524

525

526

527528

529

530531

532

533

534

535

536

537

538539

540

541542543

544545

This work was supported by the Department of Energy Office of Science grant number DE-SC0019065 and NSF grant number 2301377. Preparation of CBM3-488 was supported as part of the Center for Lignocellulose Structure and Formation, an Energy Frontier Research Center funded by the US Department of Energy, Office of Science, Basic Energy Sciences under award DE-SC0001090. Cel7A catalytic domain protein was generously provided by Stephen R. Decker, National Renewable Energy Laboratory (NREL).

References

- Y. Nishiyama, P. Langan, H. Chanzy, Crystal structure and hydrogen-bonding system in cellulose Iβ from synchrotron X-ray and neutron fiber diffraction. *Journal of the American Chemical Society* 124, 9074-9082 (2002).
- 549 2. C. M. Payne et al., Fungal cellulases. Chemical reviews 115, 1308-1448 (2015).
- 550 3. B. S, Trichoderma reesei cellulases. *Trends in biotechnology* 1, 156-161 (1983).
- 551 4. R. Wolfenden, X. Lu, G. Young, Spontaneous hydrolysis of glycosides. *Journal of the American Chemical Society* **120**, 6814-6815 (1998).
- 5. R. Wolfenden, M. J. Snider, The depth of chemical time and the power of enzymes as catalysts.

 Accounts of chemical research **34**, 938-945 (2001).
- 555 6. J. Kari *et al.*, Kinetics of cellobiohydrolase (Cel7A) variants with lowered substrate affinity.
 556 *Journal of Biological Chemistry* **289**, 32459-32468 (2014).
- 557 7. A. Nakamura *et al.*, The tryptophan residue at the active site tunnel entrance of Trichoderma 558 reesei cellobiohydrolase Cel7A is important for initiation of degradation of crystalline cellulose. 559 *The Journal of biological chemistry* **288**, 13503-13510 (2013).
- 560 8. J. Ståhlberg et al., Activity studies and crystal structures of catalytically deficient mutants of

- cellobiohydrolase I fromTrichoderma reesei. *Journal of molecular biology* **264**, 337-349 (1996).
- 562 9. G. Zou *et al.*, Alleviating product inhibition of Trichoderma reesei cellulase complex with a product-activated mushroom endoglucanase. *Bioresource technology* **319**, 124119 (2021).
- 564 10. S.-S. Han *et al.*, Engineering of the Conformational Dynamics of an Enzyme for Relieving the Product Inhibition. *ACS Catalysis* **6**, 8440-8445 (2016).
- 566 11. M. E. Atreya, K. L. Strobel, D. S. Clark, Alleviating product inhibition in cellulase enzyme Cel7A.

 Biotechnology and bioengineering 113, 330-338 (2016).
- 568 12. H. J. Gilbert, The biochemistry and structural biology of plant cell wall deconstruction. *Plant physiology* **153**, 444-455 (2010).
- 570 13. T. Jeoh *et al.*, Cellulase digestibility of pretreated biomass is limited by cellulose accessibility.
 571 *Biotechnology and bioengineering* **98**, 112-122 (2007).
- 572 14. M. Gruno, P. Väljamäe, G. Pettersson, G. Johansson, Inhibition of the Trichoderma reesei cellulases by cellobiose is strongly dependent on the nature of the substrate. *Biotechnology* and bioengineering **86**, 503-511 (2004).
- 575 **15. Z.** Yue, W. Bin, Y. Baixu, G. Peiji, Mechanism of cellobiose inhibition in cellulose hydrolysis by cellobiohydrolase. *Science in China. Series C, Life sciences* **47**, 18-24 (2004).
- 577 16. J. Ståhlberg, G. Johansson, G. Pettersson, A new model for enzymatic hydrolysis of cellulose based on the two-domain structure of cellobiohydrolase I. *Bio/Technology* **9**, 286-290 (1991).
- 579 **17**. M. Holtzapple, M. Cognata, Y. Shu, C. Hendrickson, Inhibition of Trichoderma reesei cellulase by sugars and solvents. *Biotechnology and bioengineering* **36**, 275-287 (1990).
- 581 18. P. Andrić, A. S. Meyer, P. A. Jensen, K. Dam-Johansen, Reactor design for minimizing product 582 inhibition during enzymatic lignocellulose hydrolysis: I. Significance and mechanism of 583 cellobiose and glucose inhibition on cellulolytic enzymes. *Biotechnology advances* **28**, 308-324 584 (2010).
- 585 19. Y. Zhao, B. Wu, B. Yan, P. Gao, Mechanism of cellobiose inhibition in cellulose hydrolysis by cellobiohydrolase. *Science in China Series C: Life Sciences* **47**, 18-24 (2004).
- 587 20. C. Divne, J. Ståhlberg, T. T. Teeri, T. A. Jones, High-resolution crystal structures reveal how a cellulose chain is bound in the 50 Å long tunnel of cellobiohydrolase I from Trichoderma reesei.

 Journal of molecular biology **275**, 309-325 (1998).
- 590 21. B. C. Knott *et al.*, The mechanism of cellulose hydrolysis by a two-step, retaining cellobiohydrolase elucidated by structural and transition path sampling studies. *Journal of the American Chemical Society* **136**, 321-329 (2014).
- 593 22. L. Bu *et al.*, Probing carbohydrate product expulsion from a processive cellulase with multiple 594 absolute binding free energy methods. *Journal of Biological Chemistry* **286**, 18161-18169 595 (2011).
- 596 23. H. Teugjas, P. Väljamäe, Product inhibition of cellulases studied with 14 C-labeled cellulose substrates. *Biotechnology for biofuels* **6**, 1-14 (2013).
- 598 24. L. Murphy et al., Product inhibition of five Hypocrea jecorina cellulases. *Enzyme and microbial technology* **52**, 163-169 (2013).
- Y. H. Lee, L. Fan, Kinetic studies of enzymatic hydrolysis of insoluble cellulose:(II). Analysis of extended hydrolysis times. *Biotechnology and bioengineering* **25**, 939-966 (1983).
- A. Fersht, Structure and mechanism in protein science: a guide to enzyme catalysis and protein folding (Macmillan, 1999).

- P. Tomme *et al.*, Studies of the cellulolytic system of Trichoderma reesei QM 9414: analysis of domain function in two cellobiohydrolases by limited proteolysis. *European Journal of Biochemistry* **170**, 575-581 (1988).
- K. Igarashi *et al.*, High speed atomic force microscopy visualizes processive movement of Trichoderma reesei cellobiohydrolase I on crystalline cellulose. *The Journal of biological chemistry* **284**, 36186-36190 (2009).
- 29. Z. K. Haviland *et al.*, Nanoscale dynamics of cellulose digestion by the cellobiohydrolase TrCel7A. *Journal of Biological Chemistry* **297** (2021).
- 512 30. D. Nong *et al.*, Integrated multi-wavelength microscope combining TIRFM and IRM modalities for imaging cellulases and other processive enzymes. *Biomedical Optics Express* **12**, 3253-3264 (2021).
- 615 31. L. E. Taylor *et al.*, Engineering enhanced cellobiohydrolase activity. *Nature communications* **9**, 616 1186 (2018).
- S. A. Pfaff *et al.*, Detecting the orientation of newly-deposited crystalline cellulose with fluorescent CBM3. *The Cell Surface* **8**, 100089 (2022).
- S. K. Brady, S. Sreelatha, Y. Feng, S. P. Chundawat, M. J. Lang, Cellobiohydrolase 1 from
 Trichoderma reesei degrades cellulose in single cellobiose steps. *Nature communications* 6,
 10149 (2015).
- 34. J. D. Lawson, E. Pate, I. Rayment, R. G. Yount, Molecular dynamics analysis of structural factors influencing back door pi release in myosin. *Biophysical journal* **86**, 3794-3803 (2004).
- 624 35. C. Kronman, A. Ordentlich, D. Barak, B. Velan, A. Shafferman, The "back door" hypothesis for product clearance in acetylcholinesterase challenged by site-directed mutagenesis. *Journal of Biological Chemistry* **269**, 27819-27822 (1994).
- W. Wriggers, K. Schulten, Investigating a back door mechanism of actin phosphate release by steered molecular dynamics. *Proteins: Structure, Function, and Bioinformatics* **35**, 262-273 (1999).
- 630 37. B. B. Hallac, A. J. Ragauskas, Analyzing cellulose degree of polymerization and its relevancy to cellulosic ethanol. *Biofuels, Bioproducts and Biorefining* **5**, 215-225 (2011).
- 632 38. M. Kurašin, P. Väljamäe, Processivity of cellobiohydrolases is limited by the substrate. *Journal of Biological Chemistry* **286**, 169-177 (2011).
- 634 39. K. Igarashi *et al.*, Traffic jams reduce hydrolytic efficiency of cellulase on cellulose surface.
 635 *Science* **333**, 1279-1282 (2011).
- 40. J. V. Vermaas *et al.*, The dissociation mechanism of processive cellulases. *Proceedings of the National Academy of Sciences* **116**, 23061-23067 (2019).
- T. D. Pollard, E. M. De La Cruz, Take advantage of time in your experiments: a guide to simple, informative kinetics assays. *Molecular biology of the cell* **24**, 1103-1110 (2013).
- 640 42. N. Rojel *et al.*, Substrate binding in the processive cellulase Cel7A: Transition state of complexation and roles of conserved tryptophan residues. *The Journal of biological chemistry* **295**, 1454-1463 (2020).

Supplementary Information

Model for Cel7A binding to immobilized cellulose

To analyze the Cel7A binding kinetics to immobilized cellulose, we developed a simple kinetic model as follows.

$$Cel7A_{free} + Cellulose \leftrightarrow Cel7A_{bound}$$

Based on this model:

$$\frac{d[Cel7A_{bound}]}{dt} = k_{on}[Cel7A_{free}][Cellulose] - k_{off}[Cel7A_{bound}]$$
 (1)

If both Cel7A and cellulose are large relative to the number of Cel7A bound to the surface, then this simplifies the equations. This condition is equivalent to saying there is no depletion of either [Cel7A_{free}] or [cellulose] due increasing [Cel7A_{bound}] over time, which can be justified as follows.

Cel7A binding in Fig. 2 is shown as number of Qdot-labeled Cel7A molecules per field of view, normalized to the fraction of the field of view taken up by immobilized cellulose. The field of view of our camera is 1200x1200 pixels at 73 nm/pixel, which comes out to 7674 μ m². From Fig. 2A, using a 0.5 nM concentration of Qdots in solution, the maximum steady-state accumulation was ~1000 Qdots per screen. This corresponds to a density of 0.13 Qdot per μ m². To determine whether this degree of binding will deplete the Qdot-labeled Cel7A from solution, we consider a 1 μ m² area of the surface and the corresponding volume above it in the ~100 μ m thick flow cell. The corresponding volume is 100 μ m³ = 10⁻¹³ L. Using Avogadro's number, a 0.5 nM Qdot concentration in this volume of solution contains (5 x 10⁻¹⁰ mol/L) *(10⁻¹³ L) *(6 x 10²³ particles/mol) = 30 particles. Binding of 0.13 Qdot per μ m² corresponds to <0.5% depletion. Thus, we can make the assumption that despite Qdot-labeled Cel7A binding to the surface, the solution concentration of Qdots remains approximately constant.

Cellulose is adsorbed to the cover glass surface by spreading 20 μ L of 2.54 mM cellulose stock solution (expressed as concentration of glucose subunits) over roughly a 1 cm² area of a coverslip. Assuming that all of the cellulose is adsorbed to the surface, this comes out to 5 x 10⁻⁸ mol of cellulose spread over 10⁸ μ m² surface area, for a surface density of 5 x 10⁻¹⁶ mol/ μ m² or 3 x 10⁸ glucose molecules/ μ m². We previously measured our bacterial cellulose to consist of one reducing end per 300 glucose subunits (1). This means that in a 1 μ m² area on the coverslip surface, there are 10⁶ reducing ends. As described above, the maximum steady state density is 0.13 Qdots/ μ m². Thus, as long as at least one in every 10⁵ reducing ends are exposed, then there will be negligible (<2%) depletion of cellulose reducing ends by bound Cel7A.

Based on these analyses, we conclude that in our assays, binding of Qdot-labeled Cel7A to surface-immobilized cellulose depletes neither the Qdot concentration in solution nor the reducing end binding sites on the surface. This allows for the simplification:

$$\frac{d[Cel7A_{bound}]}{dt} = k_{on}[Cel7A_{total}][Cellulose_{total}] - k_{off}[Cel7A_{bound}]$$
 (2)

At steady-state, the time derivative goes to zero, hence:

$$[Cel7A_{bound}]_{SS} = \frac{k_{on}[Cel7A_{total}][Cellulose_{total}]}{k_{off}}$$
(3)

Using the initial condition of zero Cel7A bound at time zero, the solution to the differential equation is an exponential rise to the steady-state with rate constant k_{off} (2):

$$[Cel7_{bound}](t) = \frac{k_{on}[Cel7A_{total}][Cellulose_{total}]}{k_{off}} (1 - e^{-k_{off}t})$$
(4)

Predicting rates of cellulose degradation in bulk assays

We can use the single-molecule results to predict expected results for cellobiose inhibition of Cel7A in bulk cellulose degradation assays. For approximating k_{cat} , if we assume a 1 nm displacement per cellobiose released (3), then based on the velocity data in Fig. 3E, the k_{cat} can be modeled as:

$$k_{cat} = 0.7 \, s^{-1} + \frac{2.1 \, s^{-1}}{1 + \frac{[cellobiose]}{2.3 \, mM}} \tag{5}$$

For approximating the K_M , we can use the steady state Cel7A accumulation results from Fig. 2C, which gives a measure of the relative enzyme affinity for cellulose as a function of [cellobiose]. From Eq. 3,

$$[Cel7A_{bound}]_{SS} \propto \frac{k_{on}}{k_{off}} = \frac{1}{K_D}$$
 (6)

Hence, if we use the K_D as a proxy for the K_M , then:

$$K_{M} \propto 1 + \frac{[cellobiose]}{2.1 \, mM} \tag{7}$$

These results are plotted below.

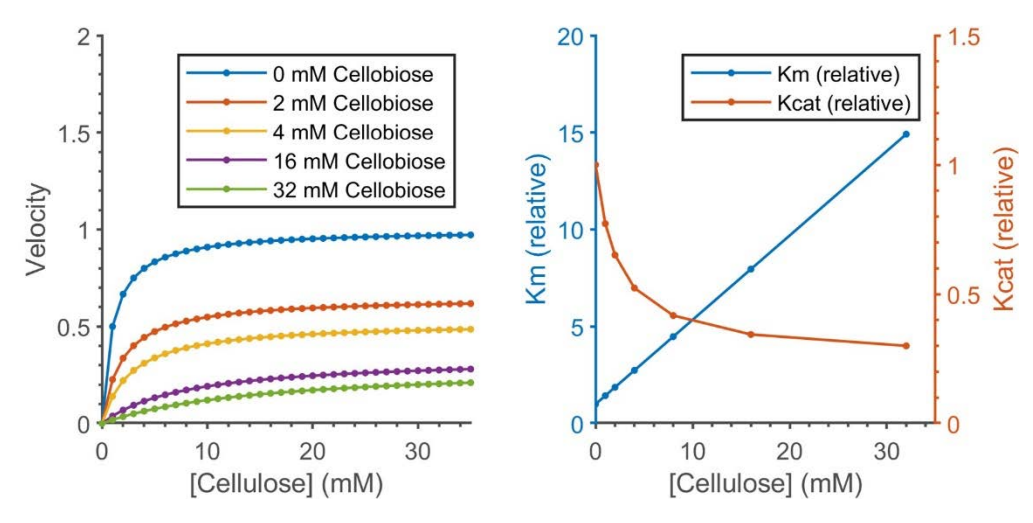


Figure SI 1: Cellulose degradation prediction in bulk assays under the presence of cellobiose. Maximum velocity (k_{cat}) and K_M are both normalized to 1 under control (no cellobiose) conditions.

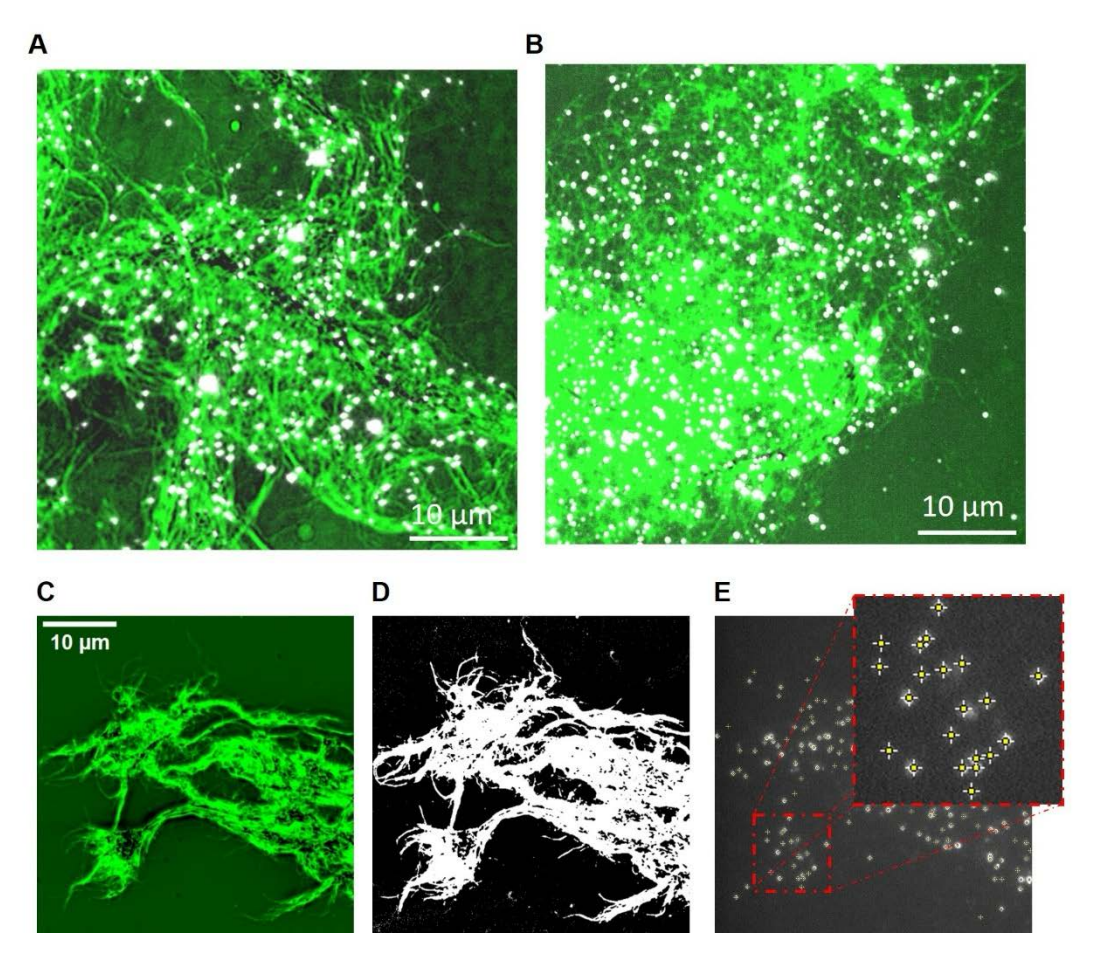


Figure SI 2: Methodology for measuring number of binding events per cellulose area. Overlaid IRM and TIRFM image of Qdot-labeled Cel7A (A) and Qdot-labeled Cel7ACD (B) (white dots) bound to immobilized cellulose (highlighted in green). To calculate the relative area of the screen occupied by cellulose, a threshold was applied using the FIJI plugin to measure the cellulose area (C and D) and the fraction of pixels above threshold was used as the fractional coverage of cellulose on the surface. (E) The number of bound enzymes was quantified using the "Find Maxima" plugin in FIJI (inset). For comparison between experiments the number of bound enzyme molecules per screen was normalized to the fraction of the area occupied by cellulose.

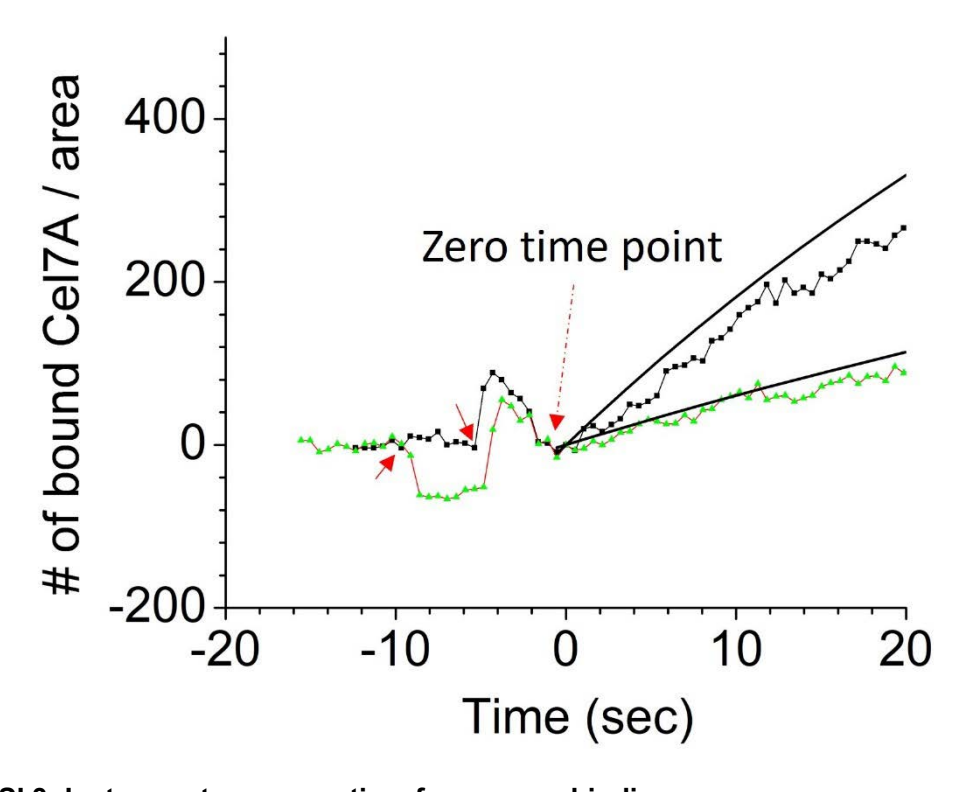


Figure SI 3: Instrument response time for enzyme binding assay.

The number of bound enzymes is shown during solution exchange of Qdot-labeled Cel7A into the flow cell. The interruptions caused by reagent exchange are indicated by the red arrows. The number of bound Cel7A is corrected by subtracting the baseline, which includes the stationary Tetraspeck beads and some auto-fluorescence of cellulose, before reagent exchange.

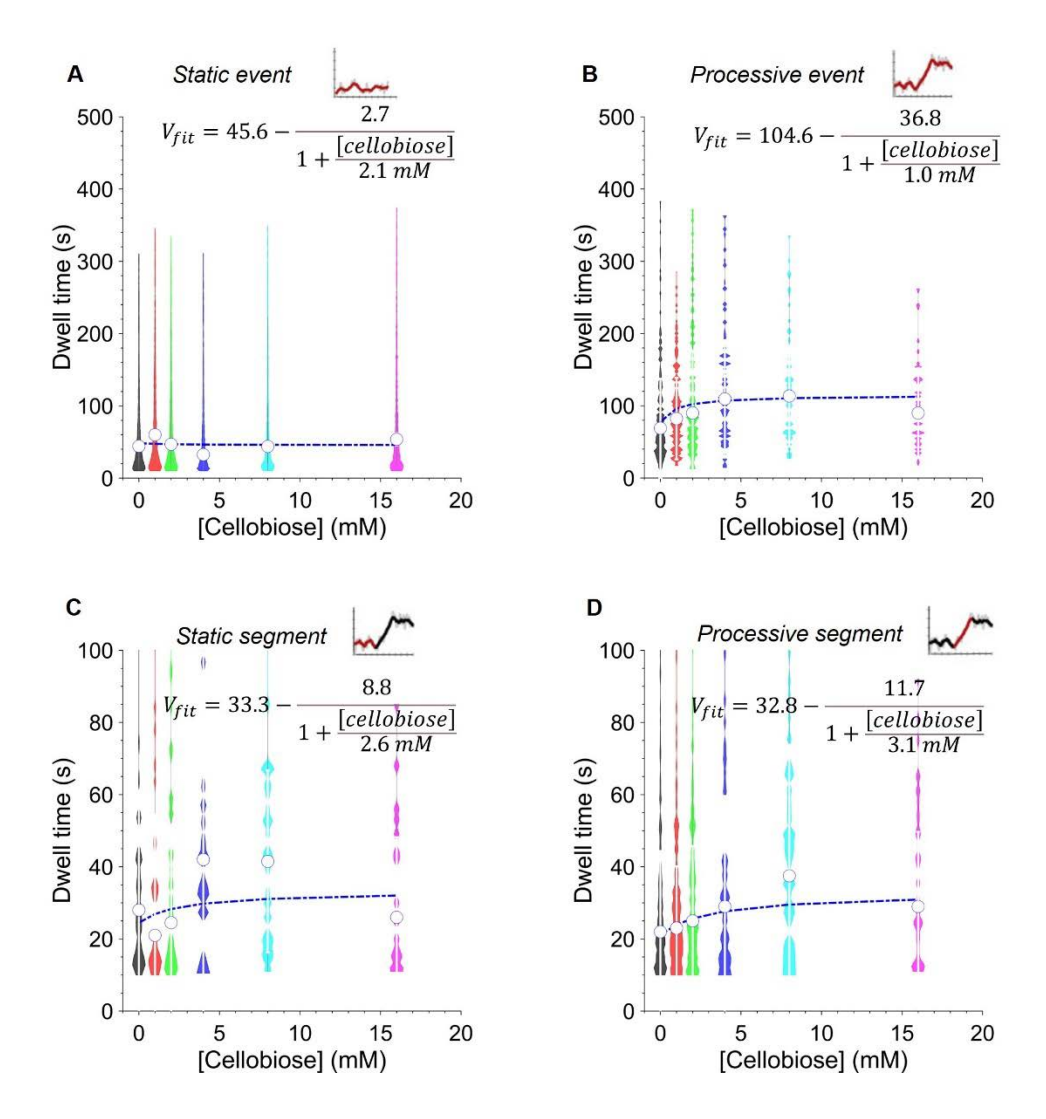


Figure SI 4: Effect of cellobiose on dwell times of isolated Cel7A CD in different phases of engagement with cellulose.

A) Dwell times of Cel7A CD static binding events, defined as binding events of duration ≥10 s with displacement <10 nm. B) Dwell times of processive events, defined as landing events that contain at least one processive segment with displacement >10 nm over at least 10 s. C) Dwell times of processive segments, with dwell time calculated as run length/velocity. D) Dwell times of static segments that occurred before or after processive segments during processive events. All plots show populations with median values as open circles except for in panel A, where the open circles indicate the mean value calculated from exponential fitting. Insets show schematic of the distance from origin versus time, with the segments of interest highlighted in red. Curves were fit to a product inhibition model in which cellobiose elongates the dwell times.

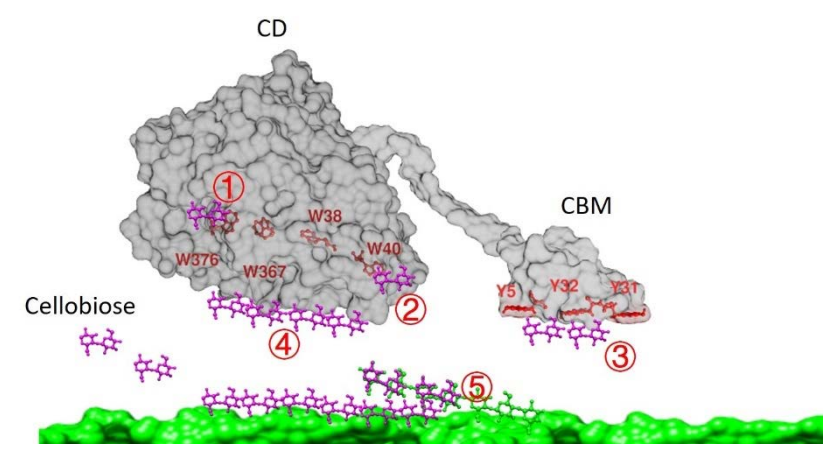


Figure SI 5: Potential sites of action of cellobiose in inhibiting Cel7A landing rate on cellulose.

As described in the Discussion, cellobiose could in principle inhibit Cel7A binding to cellulose by binding to 1) the product release site (back door), 2) the substrate binding tunnel (front door), 3) the carbohydrate binding module, 4) a cryptic site on the catalytic domain, or 5) by binding directly to cellulose.

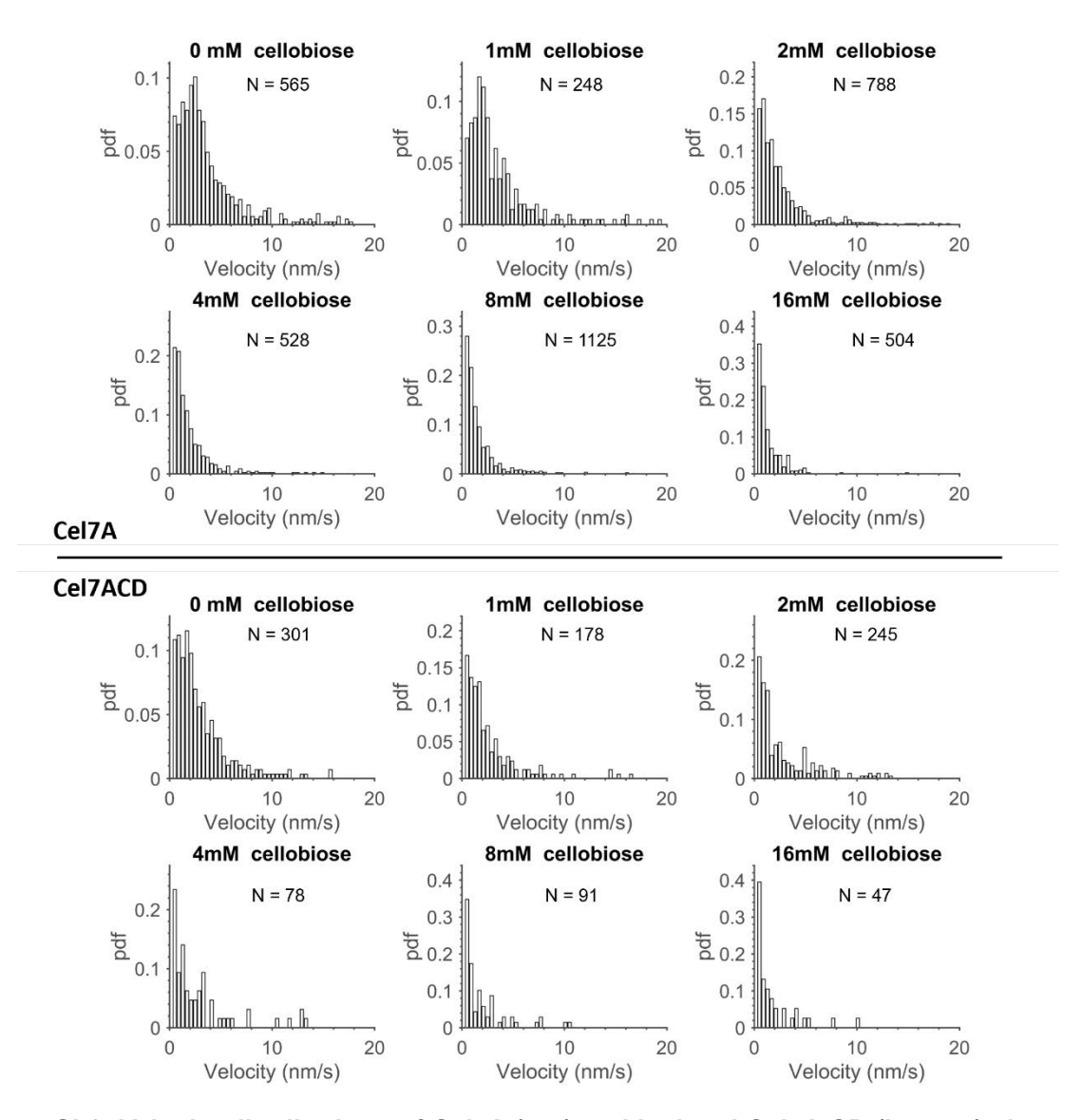


Figure SI 6: Velocity distributions of Cel7A (top) and isolated Cel7A CD (bottom) shown in Figure 3E and 3G.

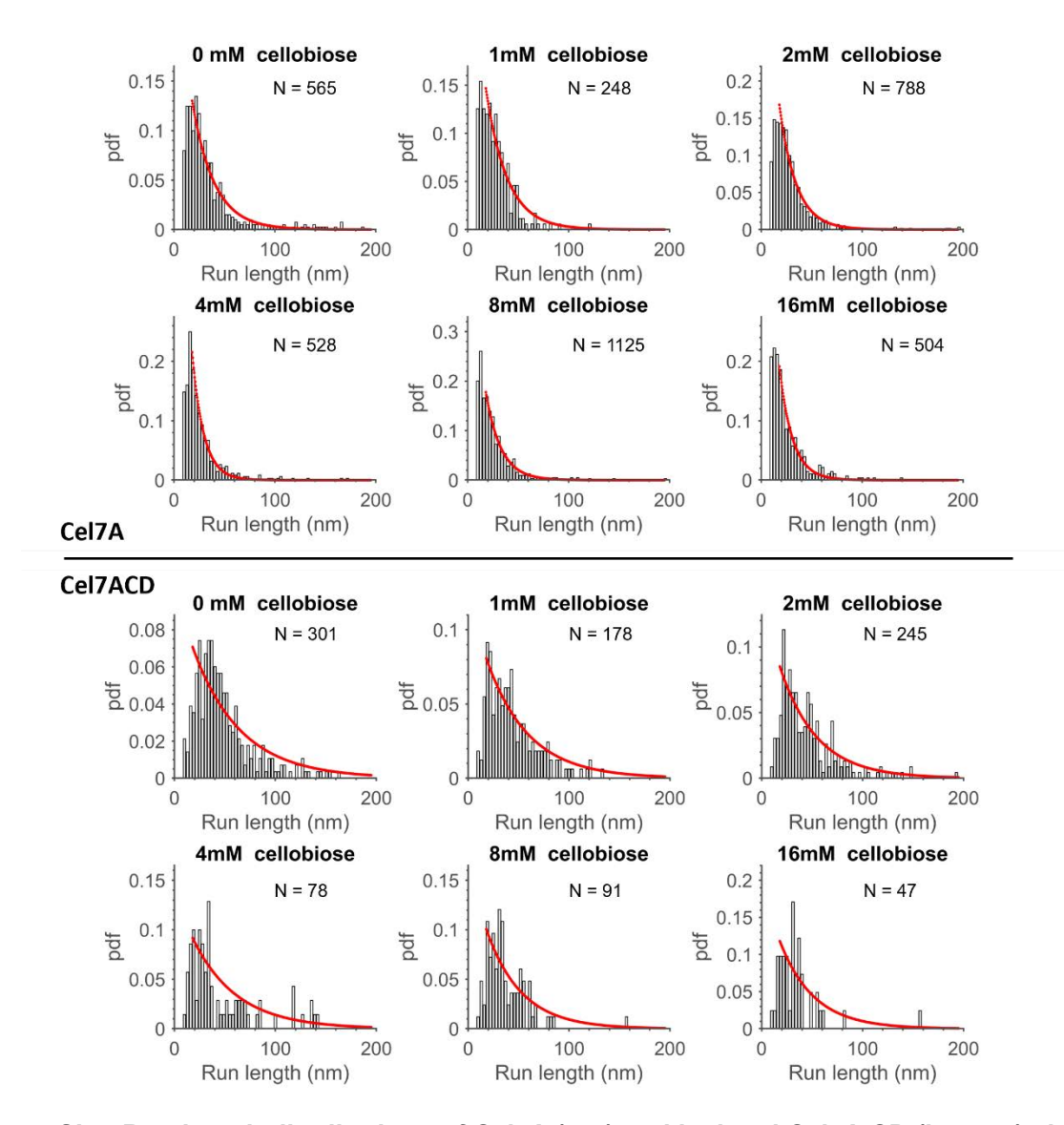


Figure SI 7: Run length distributions of Cel7A (top) and isolated Cel7A CD (bottom) shown in Figure 3F and 3H, with exponential fits (red).

Fitting of run length	Figure SI 7				
Equation					
		$A*(1-\exp(-k_{obs}*x))$ Cel7A		C	el7ACD
[Cellobiose]		Value	95% confidence interval	Value	95% confidence interval
Control 0mM	Α	0.2978	[0.2399,0.3558]	0.1038	[0.0756,0.1320]
Control offici	k _{obs}	0.04598	[0.0394,0.0526]	0.02132	[0.0152,0.0275]
1mM	Α	0.3456	[0.2552,0.4360]	0.1249	[0.1027,0.1471]
TITIIVI	kobs	0.04755	[0.0383,0.0568]	0.02422	[0.0198,0.0287]
2mM	Α	0.4972	[0.4137,0.5806]	0.1391	[0.1070,0.1713]
ZITIIVI	kobs	0.06025	[0.0538,0.0667]	0.02734	[0.0213,0.0334]
4mM	Α	1.039	[0.8330,1.2450]	0.1386	[0.0790,0.1983]
4111101	kobs	0.08744	[0.0788,0.0960]	0.02294	[0.0116,0.0343]
8mM	Α	0.5941	[0.4995,0.6887]	0.1694	[0.0829,0.2559]
OITIIVI	kobs	0.06708	[0.0608,0.0734]	0.02898	[0.0143,0.0437]
16mM	Α	0.7593	[0.5662,0.9524]	0.2018	[0.0809,0.3228]
TOLLINI	kobs	0.07656	[0.0660,0.0871]	0.02981	[0.0110,0.0487]

Table SI 1: Exponential fit parameters for run length distributions in Figure SI 7.

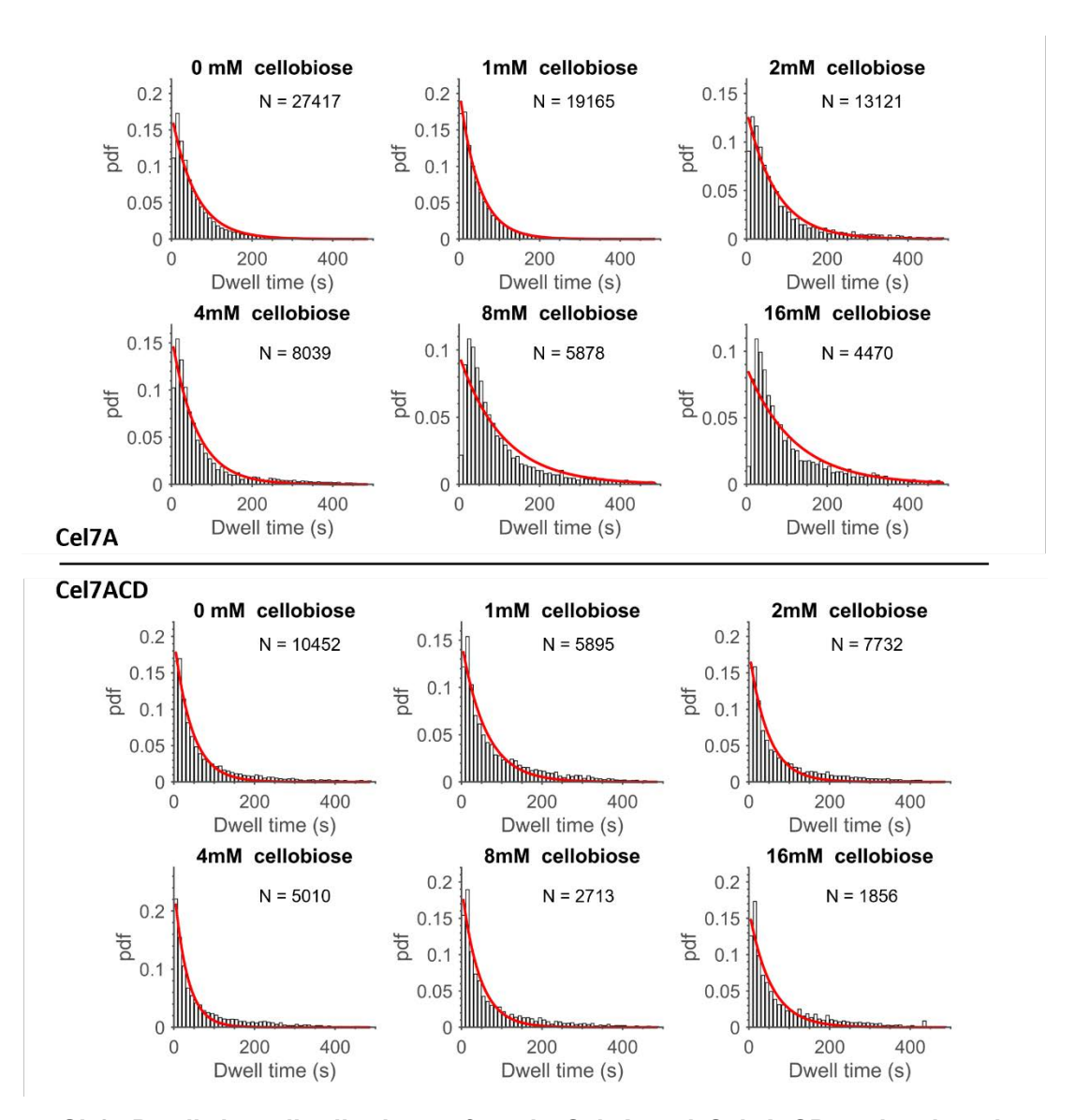


Figure SI 8: Dwell time distributions of static Cel7A and Cel7A CD molecules shown in Figure 4A, with exponential fits (red).

Fitting of static event	Figure SI 8						
Equation		$A*(1-\exp\left(-k_{obs}*x\right))$					
	Cel7A		C	el7ACD			
[Cellobiose]		Value	95% confidence interval	Value	95% confidence interval		
Control 0mM	Α	0.1724	[0.1558,0.1889]	0.1989	[0.1865,0.2112]		
Control omivi	k_{obs}	0.01691	[0.0146,0.0192]	0.0226	[0.0206,0.0246]		
1mM	Α	0.2095	[0.2004,0.2187]	0.1493	[0.1364,0.1622]		
TIMINI	k_{obs}	0.02095	[0.0197,0.0222]	0.01665	[0.0146,0.0187]		
2mM	Α	0.1335	[0.1226,0.1443]	0.1823	[0.1690,0.1956]		
Zmivi	k_{obs}	0.01363	[0.0121,0.0152]	0.02129	[0.0191,0.0235]		
4mM	Α	0.1575	[0.1421,0.1730]	0.2459	[0.2299,0.2619]		
4mivi	k_{obs}	0.01621	[0.0140,0.0185]	0.03069	[0.0279,0.0335]		
O N 4	А	0.09652	[0.0800,0.1130]	0.1963	[0.1769,0.2156]		
8mM	k_{obs}	0.009235	[0.0070,0.0115]	0.02277	[0.0196,0.0259]		
16mM	Α	0.08799	[0.0717,0.1043]	0.1623	[0.1450,0.1795]		
TOLLINI	k_{obs}	0.008499	[0.0063,0.0107]	0.0186	[0.0158,0.0214]		

Table SI 2: Exponential fit parameters of static dwell time distributions in Figure SI 8.

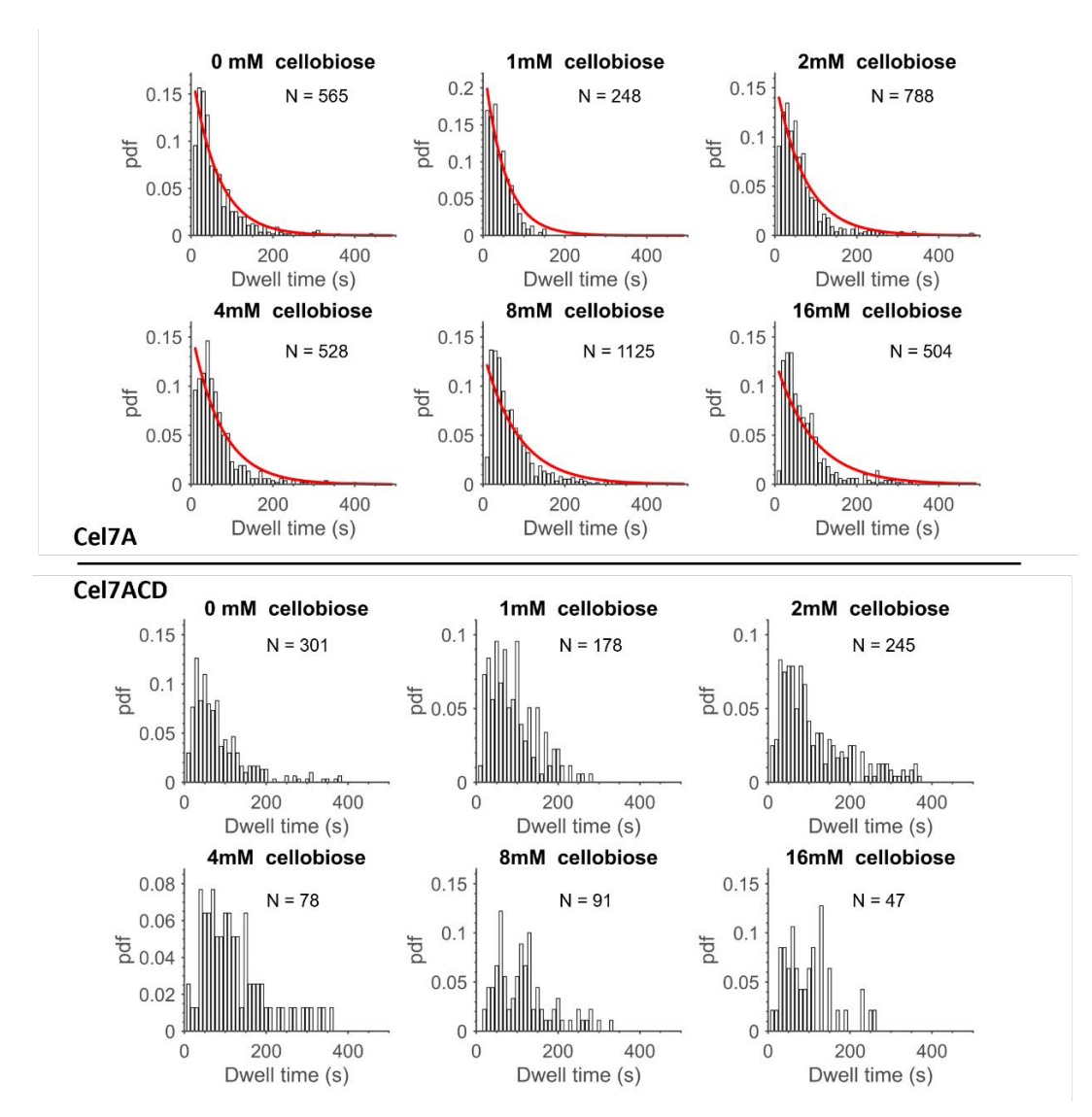


Figure SI 9: Dwell time distribution of processive Cel7A and Cel7A CD shown in Figure 4B. Cel7A include exponential fits, but due to sparsity of data, fits are omitted for Cel7A CD.

Fitting of processive 6	Figure SI 9		
Equation		$A * (1 - \exp(-k_a))$	obs * x))
			Cel7A
[Cellobiose]		Value	95% confidence interval
Control 0mM	Α	0.1786	[0.1470,0.2102]
Control offily	k _{obs}	0.01576	[0.0121,0.0194]
1mM	Α	0.2415	[0.1938,0.2892]
TIIIIVI	k _{obs}	0.0196	[0.0144,0.0248]
2mM	Α	0.161	[0.1347,0.1873]
Zmivi	k _{obs}	0.01399	[0.0109,0.0170]
4mM	Α	0.1586	[0.1292,0.1879]
4111101	kobs	0.01368	[0.0103,0.0170]
8mM	Α	0.1362	[0.1042,0.1682]
OITIVI	k _{obs}	0.01179	[0.0081,0.0155]
16mM	Α	0.1276	[0.0898,0.1654]
TOUNIAL	kobs	0.01087	[0.0065,0.0153]

Table SI 3: Exponential fit parameters of processive dwell time distributions in Figure SI 9.

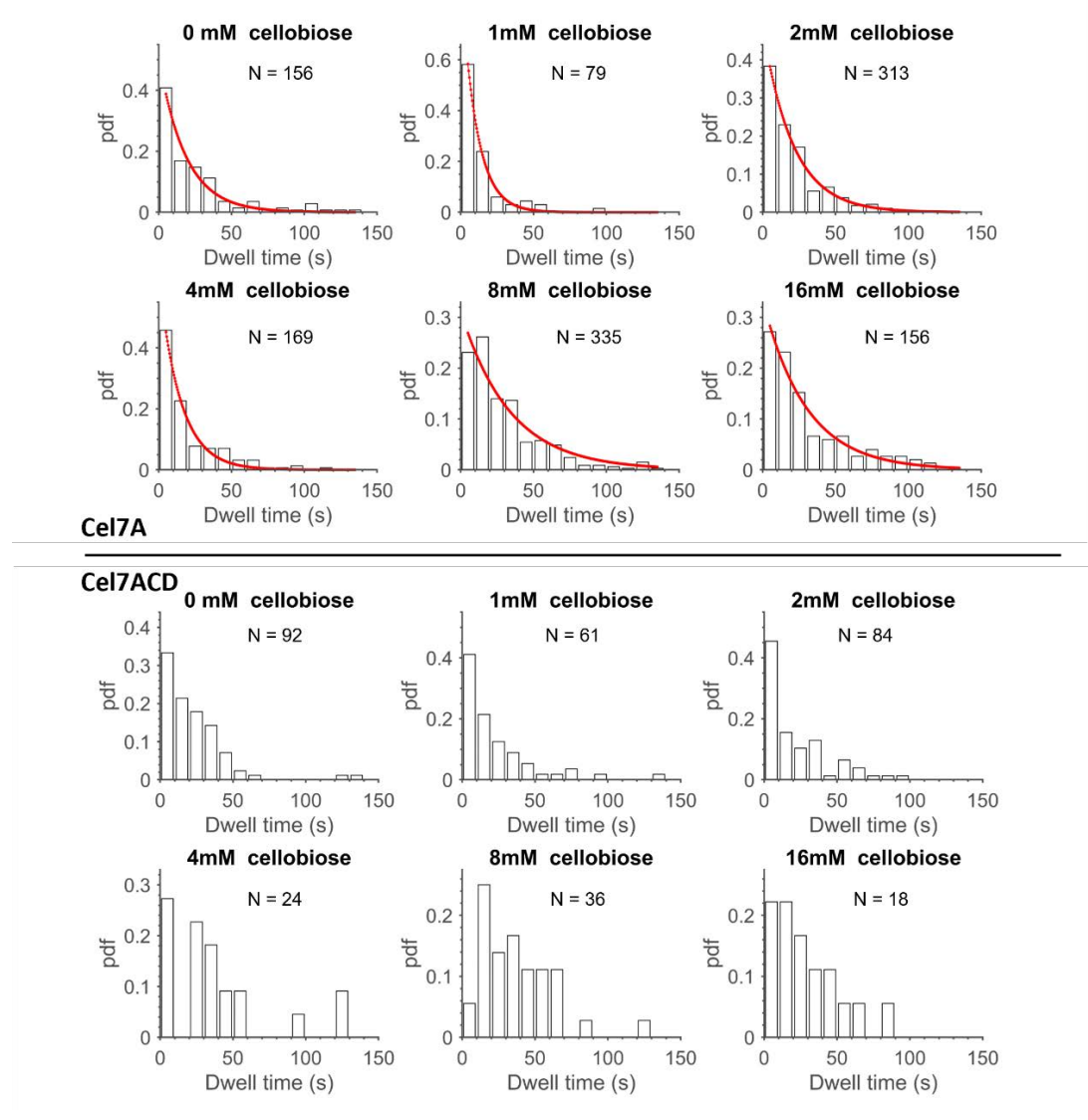


Figure SI 10: Distributions of static segment durations for processive Cel7A and Cel7A CD, shown in Figure 4C.

Fitting of static segme	Figure SI 10		
Equation		$A*(1-\exp(-k_{obs}*x))$	
			Cel7A
[Cellobiose]		Value	95% confidence interval
Control 0mM	Α	0.5093	[0.4249,0.5938]
Control offlivi	kobs	0.0544	[0.0420,0.0668]
1mM	Α	0.9384	[0.7770,1.1000]
TIIIVI	k _{obs}	0.05496	[0.0738,0.1161]
2mM	Α	0.4875	[0.4361,0.5388]
ZIIIVI	k _{obs}	0.04829	[0.0412,0.0553]
4mM	Α	0.6345	[0.5371,0.7319]
4111101	k _{obs}	0.06791	[0.0538,0.0820]
8mM	Α	0.3122	[0.2515,0.3729]
OITIVI	k _{obs}	0.02958	[0.0215,0.0377]
16mM	Α	0.3348	[0.2846,0.3849]
TOUNIA	kobs	0.03357	[0.0265,0.0407]

Table SI 4: Exponential fit parameters of static segment distributions in Figure SI 10.

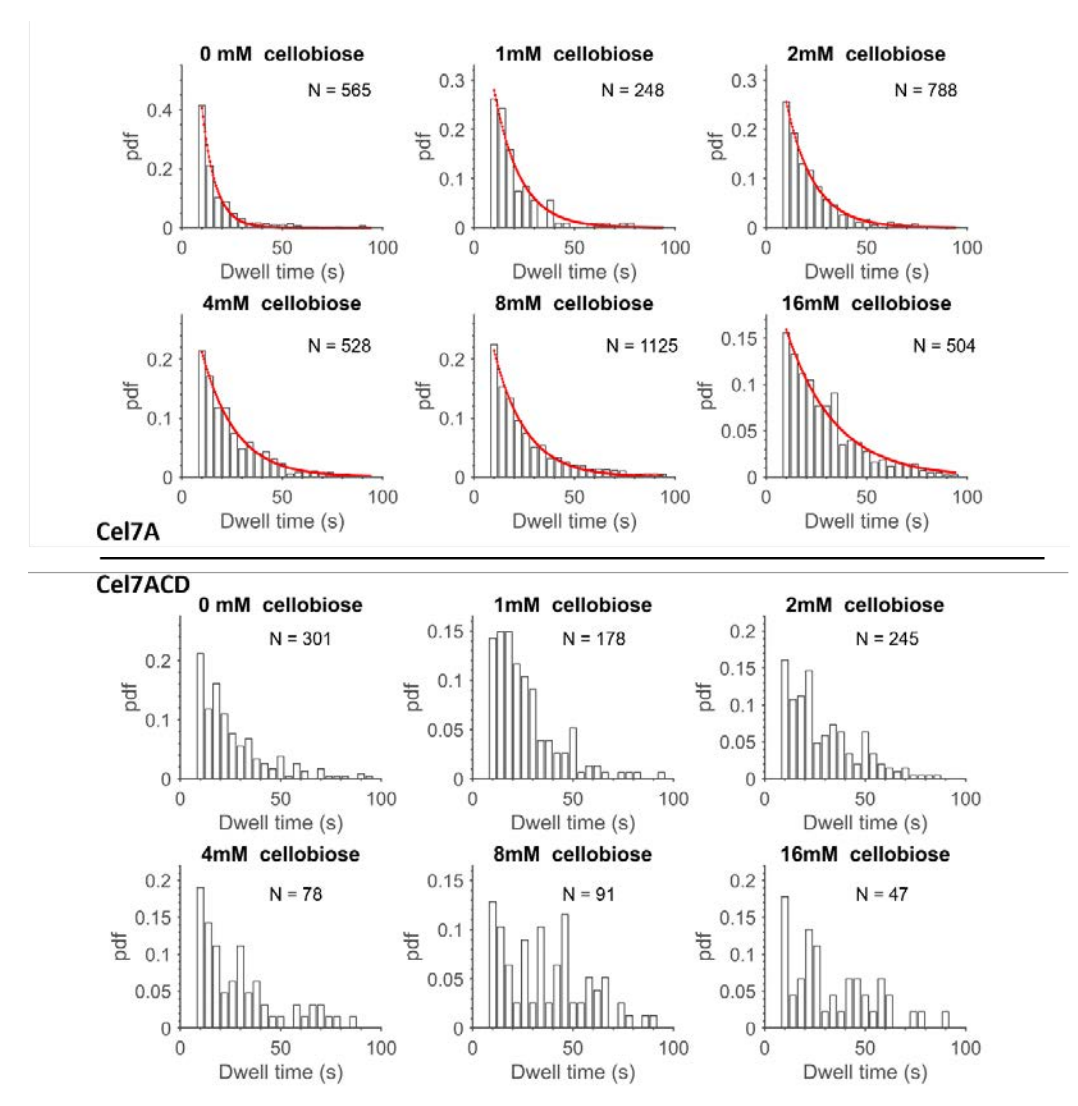


Figure SI 11: Distributions of processive segment durations for processive Cel7A and Cel7A CD, shown in Figure 4D.

Fitting of processive s	segment distr	ibution	Figure SI 11
Equation		$A * (1 - \exp(-k_{obs}))$	* x))
			Cel7A
[Cellobiose]		Value	95% confidence interval
Control 0mM	Α	1.804	[1.4530,2.1550]
Control Omivi	kobs	0.149	[0.1330,0.1650]
1 1-4	Α	0.6045	[0.4471,0.7619]
1mM	kobs	0.07699	[0.0603,0.0937]
2mM	А	0.535	[0.4946,0.5754]
ZMIVI	kobs	0.07371	[0.0691,0.0783]
4mM	Α	0.3849	[0.3433,0.4264]
4mivi	kobs	0.05967	[0.0538,0.0655]
8mM	А	0.4023	[0.3670,0.4376]
OTTIVI	kobs	0.06302	[0.0581,0.0679]
16mM	Α	0.241	[0.2113,0.2707]
16mM	kobs	0.04135	[0.0361,0.0466]

Table SI 5: Exponential fit parameters for processive segment distributions in Figure SI 11.

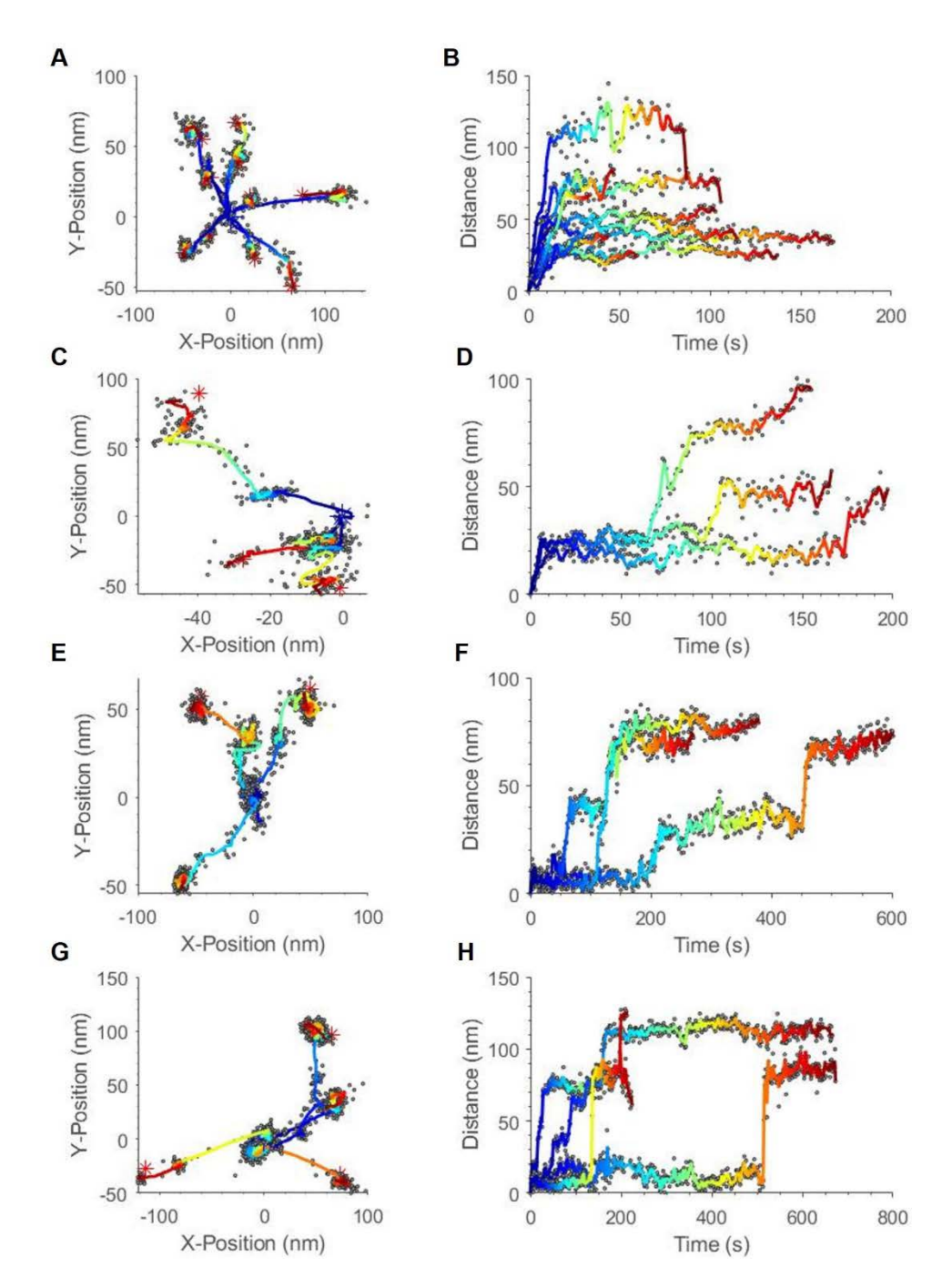


Figure SI 12: Gallery of single-molecule trajectories of Cel7A in control conditions. In the XY plots at left, the enzyme all start at point (0,0) and time of traces transitions from blue to red. Corresponding distance from origin versus time traces are shown at right.

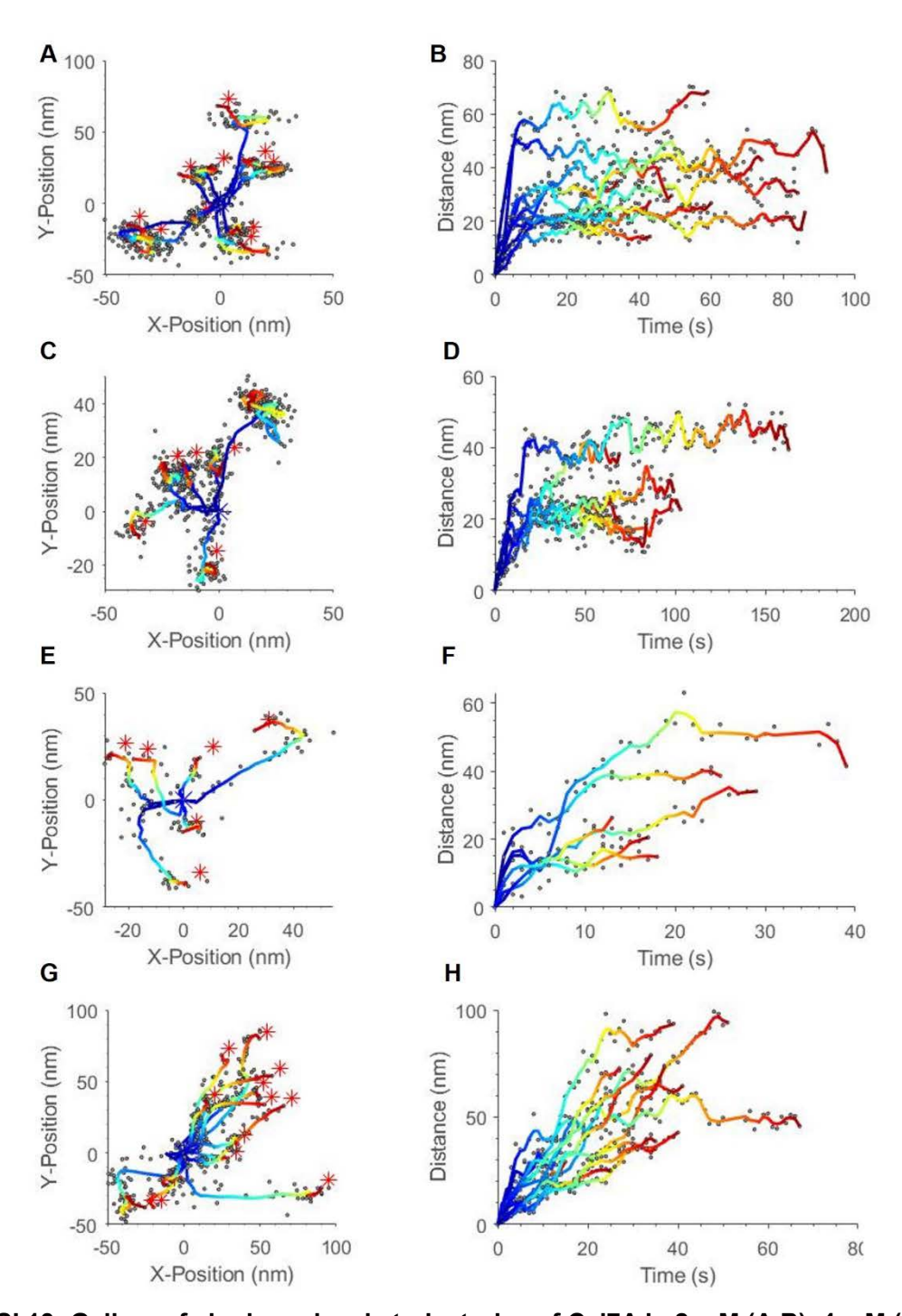


Figure SI 13: Gallery of single-molecule trajectories of CeI7A in 2 mM (A,B), 4 mM (C,D), 8 mM (E,F), and 16 mM (G,H) cellobiose.

In the XY plots at left, the enzyme all start at point (0,0) and time of traces transitions from blue to red. Corresponding distance from origin versus time traces are shown at right.

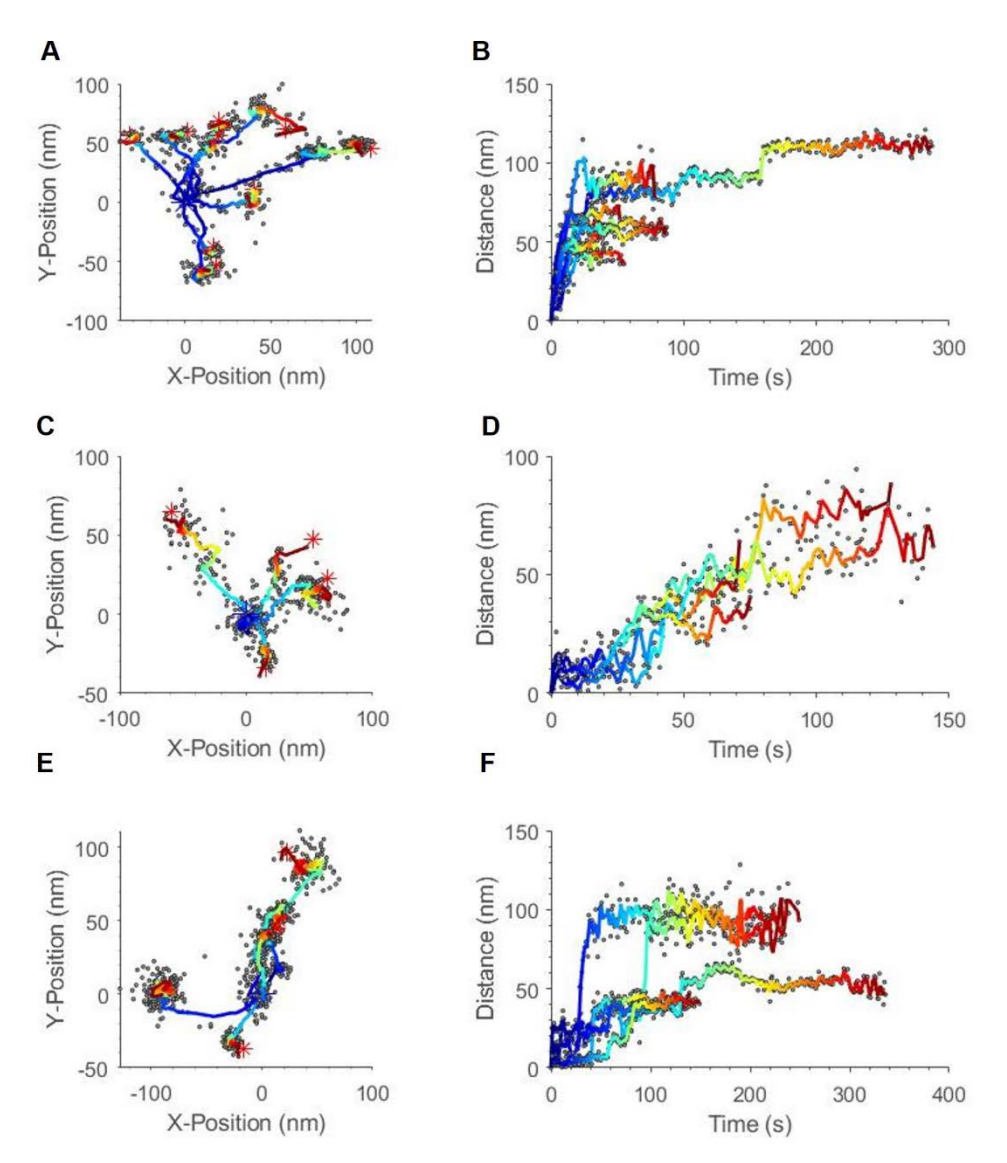


Figure SI 14: Gallery of single-molecule trajectories of Cel7A CD in control conditions. In the XY plots at left, the enzyme all start at point (0,0) and time of traces transitions from blue to red. Corresponding distance from origin versus time traces are shown at right.

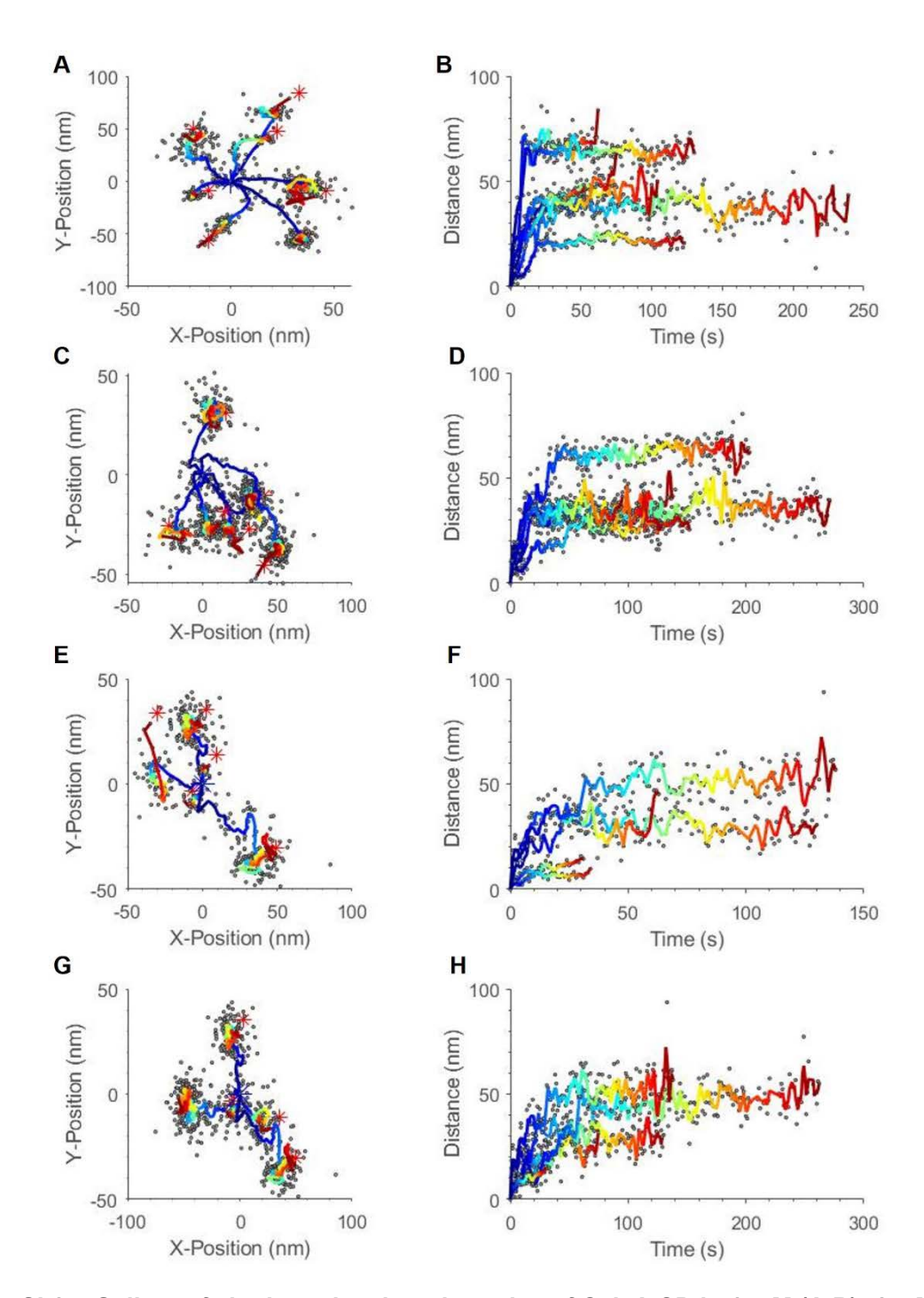


Figure SI 15: Gallery of single-molecule trajectories of Cel7A CD in 1 mM (A,B), 4 mM (C,D), 8 mM (E,F), and 16 mM (G,H) cellobiose.

In the XY plots at left, the enzyme all start at point (0,0) and time of traces transitions from blue to red. Corresponding distance from origin versus time traces are shown at right.

Binding of Cel7A and Cel7ACD in the presence of Cellobiose Fig. 2B, Fig. 2D								
Binding of Cel7A and Cel7	Binding of Cel7A and Cel7ACD in the presence of Cellobiose							
Equation		A * (1 - ex	$\operatorname{cp}\left(-k_{obs} * x\right)$					
		Cel	7A	Cel	17ACD			
[Cellobiose]		Value	Standard Error	Value	Standard Error			
Control	Α	1022.5	6.2	930.5	2.5			
Control	k_{obs}	0.01952	0.00038	0.018	0.00020			
1mM	Α	715.6	4.9	797.1	2.2			
TITIVI	k _{obs}	0.01437	0.00025	0.0232	0.00031			
2mM	Α	514.2	4.2	616.6	1.6			
ZIIIVI	k _{obs}	0.0125	0.00023	0.01504	0.00014			
4mM	Α	441.3	6.6	503.9	2.2			
4111101	k_{obs}	0.00774	0.00020	0.01671	0.00028			
8mM	Α	129.9	0.8	251.3	1.0			
OTTIVI	k _{obs}	0.03519	0.00098	0.0206	0.00035			
16mM	Α	42.4	0.8	92.4	1.6			
TOLLIM	k_{obs}	0.0264	0.0021	0.00885	0.00037			

Table SI 6: Exponential fit parameters for number of bound enzymes in Figure 2B and D.

Binding of Cel7A in the pr	resence of Cellopentaose		Fig. 6A
Equation	A * (1 − e.	$xp(-k_{obs} * x)$	
		Value	Standard Error
Control	Α	1290.7	4.8
Control	k _{obs}	0.00936	0.00009
0.5	Α	975.9	1.7
0.5 μΜ	k_{obs}	0.00972	0.00004
4 8 4	Α	655.2	4.3
1 μM	k _{obs}	0.00863	0.00013
2M	Α	214.6	1.4
2 μΜ	k_{obs}	0.02138	0.00064
4 - 14	Α	264.1	14.2
4 μΜ	k_{obs}	0.00495	0.00046

Table SI 7: Exponential fit parameters for number of bound Cel7A in Figure 6A.

Binding of CBM3 in the	presence of Cellobiose		Fig. 5C
Equation	A * (1 - e)	$xp(-k_{obs} * x)$	
		Value	Standard Error
Control	А	423.6	1.9
Control	k_{obs}	0.18293	0.0051
50 mM Cellobiose	Α	358.6	1.8
30 IIIWi Cellobiose	k_{obs}	0.21259	0.00711
50 μM Cellopenteose	А	387.8	2.3
	k_{obs}	0.1222	0.0035

Table SI 8: Exponential fit parameters for number of bound CBM in Figure 5C.

Inhibition of Cel7	'A bin <mark>din</mark> g			17	No. 140		171
Equation	\$ 8	25	у	$a_0 + A/(1 - A)$	$+x/K_I$		
	v.		Cellobiose			Cellopentaose	
	-	Cel7	Cel7A (Fig. 2C)		Cel7ACD (Fig. 2E)		A (Fig. 6B)
	₹.	Value	Standard Error	Value	Standard Error	Value	Standard Error
	Vo	0	0	0	0	0	0
	Α	1.0000	0.003	1.0000	0.0016	1332.10	133.1
	K_I	2.097	0.14	2.999	0.49	0.879	0.27

Table SI 9: Fit parameters for the inhibition of Cel7A and Cel7A CD binding by cellobiose and cellopentaose in Figures 2C, 2E, and 6B.

quation	$y_0 + A/(1 + x/K_I)$						
J-18-11010-1-1-1-1-1-1		Cel7A		Cel7ACD			
		Value	Standard Error	Value	Standard Erro		
Velocity	y _o	0.713	0.24	0.726	0.28		
	Α	2.156	0.25	1.455	0.27		
(Fig. 3E, 3G)	K_I	2.356	0.96	3.343	2.12		
Run length (Fig. 3F, 3H)	yo	11.32	3.3	32.94	5.6		
	Α	11.11	3.8	13.31	6.1		
	K_I	1.93	2.3	2.23	3.5		
Danasalias Carrant	y _o	27.21	7.3	55.68	32.9		
Processive Segment	Α	-19.12	6.7	-38.50	30.2		
(Fig.4D and Fig. SI 4D)	K_I	5.54	5.9	7.16	15.5		
Processive event	y _o	119.55	49.9	2423.38	11322.1		
	Α	-61.82	46.9	-2299.50	11296.2		
(Fig.4B and Fig. SI 4B)	K_I	11.91	19.9	100.00	572.3		
Static event	y _o	224.03	238.8	45.61	16.1		
The second secon	Α	-172.46	232.6	2.75	17.8		
(Fig.4A and Fig. SI 4A)	K_I	23.67	52.8	2.11	47.5		
Static cogmont	yo	50.46	68.6	87.44	71.0		
Static segment	A	-36.40	65.6	-72.60	67.1		
(Fig.4C and Fig. SI 4C)	K_I	16.11	56.0	4.22	12.7		

Table SI 10: Fit parameters for the inhibition of Cel7A and Cel7ACD motility by cellobiose in Figures 3, 4, and SI 4.

References

- 1. Z. K. Haviland *et al.*, Nanoscale dynamics of cellulose digestion by the cellobiohydrolase TrCel7A. *Journal of Biological Chemistry* **297** (2021)
- 2. S. R. Hoare, Analyzing kinetic binding data. Assay Guidance Manual [Internet] (2021).
- 3. S. K. Brady, S. Sreelatha, Y. Feng, S. P. Chundawat, M. J. Lang, Cellobiohydrolase 1 from

Trichoderma reesei degrades cellulose in single cellobiose steps. Nature communications **6**, 10149 (2015)